



**HAL**  
open science

**Elucidating heterogeneous nitrate contamination in a small basement aquifer. A multidisciplinary approach: NO<sub>3</sub> isotopes, CFCs-SF<sub>6</sub>, microbiological activity, geophysics and hydrogeology**

Emmanuelle Petelet-Giraud, Nicole Baran, V. Vergnaud-Ayraud, Angélie Portal, C. Michel, Catherine Joulian, F. Lucassou

► **To cite this version:**

Emmanuelle Petelet-Giraud, Nicole Baran, V. Vergnaud-Ayraud, Angélie Portal, C. Michel, et al.. Elucidating heterogeneous nitrate contamination in a small basement aquifer. A multidisciplinary approach: NO<sub>3</sub> isotopes, CFCs-SF<sub>6</sub>, microbiological activity, geophysics and hydrogeology. Journal of Contaminant Hydrology, 2021, 241, pp.103813. 10.1016/j.jconhyd.2021.103813 . hal-03336986

**HAL Id: hal-03336986**

**<https://hal.science/hal-03336986v1>**

Submitted on 9 May 2023

**HAL** is a multi-disciplinary open access archive for the deposit and dissemination of scientific research documents, whether they are published or not. The documents may come from teaching and research institutions in France or abroad, or from public or private research centers.

L'archive ouverte pluridisciplinaire **HAL**, est destinée au dépôt et à la diffusion de documents scientifiques de niveau recherche, publiés ou non, émanant des établissements d'enseignement et de recherche français ou étrangers, des laboratoires publics ou privés.



Distributed under a Creative Commons Attribution - NonCommercial 4.0 International License

1 **Elucidating heterogeneous nitrate contamination in a small**  
2 **basement aquifer. A multidisciplinary approach: NO<sub>3</sub> isotopes,**  
3 **CFCs-SF<sub>6</sub>, microbiological activity, geophysics and**  
4 **hydrogeology.**  
5

6 PETELET-GIRAUD Emmanuelle<sup>1</sup>, BARAN Nicole<sup>1</sup>, VERGNAUD-AYRAUD Virginie<sup>2</sup>,  
7 PORTAL Angélie<sup>1</sup>, MICHEL Caroline<sup>1</sup>, JOULIAN Catherine<sup>1</sup>, LUCASSOU Flora<sup>3</sup>

8 <sup>1</sup> BRGM, F-45060 Orléans, France

9 <sup>2</sup> OSUR, Plateforme Condate Eau, CNRS-Rennes 1 University, 35042 Rennes, France

10 <sup>3</sup> BRGM, F-35700 Rennes, France  
11

12 Corresponding author: PETELET-GIRAUD Emmanuelle, BRGM, 3 av. C Guillemin,  
13 BP36009, 45060 Orléans Cedex 2, France, Email: e.petelet@brgm.fr  
14  
15  
16

17

18

19

20

21

22

23

24

25

26

27

28

29

30

31

32

33

34

35

36

37

38

39

40

**Highlights**

- Heterogeneous nitrate groundwater contamination in a small basement-rock aquifer
- Nitrate contamination is controlled by anthropogenic activities and hydrogeology
- Past land use has a significant remanent effect on nitrate concentration in groundwater
- Dual isotope approach of NO<sub>3</sub> revealed its source and denitrification processes
- Multidisciplinary approach allows deciphering driving mechanisms of contamination

**Keywords**

Nitrate contamination, basement aquifer, nitrate isotopes, groundwater residence time, microbiological activity, Electrical Resistivity Tomography geophysics, Plourhan catchment

**Abstract**

Nitrate contamination of groundwater remains a major concern despite all the measures and efforts undertaken over the last decades to protect water resources. We focused on a small catchment in Brittany (France) facing nitrate pollution with concentrations over the European drinking water standard of 50 mg.L<sup>-1</sup>. This is a common situation in catchments where - supposedly effective - measures were applied for reducing the transfer of N to groundwater. At the scale of this small (~100 ha) basement aquifer, nitrate concentrations are very heterogeneous in the groundwater, sampled up to 15-20 m below the soil surface in several observation wells (hereafter referred as piezometers) and up to 110 m deep in a borehole drilled through a faulted area near the Spring (outlet of the catchment). We used

41 complementary and robust approaches for exploring and better to better constraining the  
42 driving parameters of nitrate transfer and distribution in groundwater. Detailed geological  
43 work and a geophysical electrical resistivity tomography survey identified the lithologies,  
44 tectonic structures and weathering layers. This highlighted a complex geological structure  
45 with several compartments delimited by faults, as well as the highly variable thickness of the  
46 weathered layer. It also illustrated the heterogeneity of the hydrosystem, some  
47 compartments appearing to be disconnected from the general groundwater flow. This was  
48 confirmed by geochemical analyses and by the mean apparent groundwater residence time  
49 based on CFCs-SF6 and noble-gas analyses, locally revealing old and nitrate-free  
50 groundwater, and very old water with a recharge temperature below than the current average  
51 temperature in the area, reflecting water dating back to the last period of glaciation (-19 to -  
52 17 ky). Nitrate isotopes clearly showed denitrification processes in a few piezometers, which  
53 was generally supported by microbiology and molecular biology results. This highlighted the  
54 presence of functional genes involved in denitrification as well as a capacity of the  
55 groundwater microbial community to denitrify when *in situ* conditions are favourable. This  
56 type of combined approach - covering chemistry, isotopic methods, dissolved gases,  
57 microbiological activity, geophysics and hydrogeology - appears to be indispensable for  
58 implementing the most relevant programme of measures and for accurately assessing their  
59 effectiveness, notably by considering the timeframe between implementation of the  
60 measures and their impact on groundwater quality.

## 61 **1 Introduction**

62 Nitrate contamination of groundwater remains a major concern despite all the efforts to  
63 protect waters aquifers against nitrate pollution, such as implementation of the European  
64 Council Directive [91/676/EEC](#) adopted in 1991, and of the European Water Framework  
65 Directive [2000/60/EC](#) and its daughter Directive [2006/118/EC](#). In addition to agronomic  
66 measures, a key issue is to arrive at better understanding the driving parameters of nitrate  
67 transfer towards, and distribution in, groundwater, i.e. the geological structures and the  
68 hydrogeological functioning.

69 The correlation between an increased use of (synthetic and organic) fertilizers and the  
70 increase of nitrate concentrations in groundwater has been known for a long time (e.g.  
71 [Aquilina et al., 2012](#)) but uncertainties remain concerning the transit time between topsoil  
72 and aquifer. In particular, the immobilization/remobilization processes of N governing  
73 nitrogen cycling and nitrate transfer through soil are still poorly constrained in terms of “delay  
74 effect”. [Sebilo et al. \(2013\)](#), who investigated the fate of a single application of an isotopically  
75 labelled nitrogen fertilizers for three decades in an experimental field, concluded that  
76 attempts for reducing agricultural nitrate contamination of aquatic systems must consider the

77 long-term legacy of past applications of synthetic fertilizer and the nitrogen-retention capacity  
78 of agricultural soils.

79 In addition to nitrogen-retention and -cycling processes in soil, the N stock – mainly nitrate –  
80 in the unsaturated aquifer zone must be considered (Baran et al., 2007). Nitrate being highly  
81 soluble, it is generally considered that it will transfer through the unsaturated zone towards  
82 groundwater at the same rate as infiltrating water. This implies that a good understanding, of  
83 the subsurface geology and its geometry as well as of the hydrogeological functioning of the  
84 aquifer system is essential, as they - at least partly - govern pollutant transfer time at the  
85 catchment scale. A proper understanding of the hydrogeological functioning can be obtained  
86 from groundwater residence-time assessment, using chlorofluorocarbons (CFCs) and  
87 sulphur hexafluoride (SF<sub>6</sub>) gases for studying modern (< 60 yr) groundwater dynamics and  
88 mixing processes. These anthropogenic gases have been released into the atmosphere  
89 since the 1950s and are now found in natural waters, with atmospheric equilibria that allow  
90 groundwater dating based on their atmospheric concentrations chronicles (e.g. Busenberg  
91 and Plummer, 1992; Ayraud et al., 2008; Aeschbach-Hertig and Solomon; 2013; Chatton et  
92 al., 2016).

93 Furthermore, part of the N can leave the nitrogen cycle as gases (N<sub>2</sub>O and N<sub>2</sub>) resulting from  
94 denitrification, governed by heterotrophic or autotrophic denitrifying bacteria transforming  
95 NO<sub>3</sub> to N<sub>2</sub> (Stein and Klotz, 2016). This process affects the global N budget, especially the  
96 nitrate one, and must be considered as a major process when evaluating of the fate of N  
97 from soil to groundwater. Nitrogen and oxygen isotopes of nitrate ( $\delta^{15}\text{N-NO}_3$  and  $\delta^{18}\text{O-NO}_3$ )  
98 are frequently used as tracers of nitrate sources in groundwater, as the various  
99 synthetic/organic N fertilizers have different isotopic compositions (Kendall et al., 2007).  
100 However, nitrate isotopes also are ideal tools for tracing N transformation processes, such as  
101 denitrification (Böttcher et al., 1990), as NO<sub>3</sub> reduction to N<sub>2</sub> is a highly fractionating process  
102 (Kendall and Aravena, 2000) leading to a joint increase of  $\delta^{15}\text{N-NO}_3$  and  $\delta^{18}\text{O-NO}_3$ , whereas  
103 simple dilution, also leading to a decrease in NO<sub>3</sub> concentration, does not modify the isotopic  
104 signatures.

105 We designed and implemented an innovative interdisciplinary study, coupling complementary  
106 and robust approaches for defining the spatio-temporal nitrate distribution in a small  
107 catchment of a basement-rock aquifer. For that purpose, we had to answer the following  
108 questions. (1) How is groundwater quality—especially for nitrate—controlled spatially and  
109 temporarily, by natural water-rock interactions and by anthropogenic input related to  
110 agricultural practises and its evolution over the past decades (hydrogeological, geophysical  
111 and chemical approaches)? (2) What are the nitrate sources and their potential attenuation,

112 as shown by N and O isotopes of NO<sub>3</sub> fingerprinting, and through assessing the  
113 denitrification potential by monitoring nitrate-reducing bacteria genes (isotopic and  
114 microbiological approaches)? (3) What is the groundwater residence-time distribution, in  
115 order to evaluate the hydrodynamics and the potential spatial variability of the aquifer, and as  
116 a supplementary constraint to support the hypothesis regarding the chemical and isotopic  
117 compositions (CFC-SF<sub>6</sub> and rare dissolved gases approach)?

118

## 119 **2 Site description**

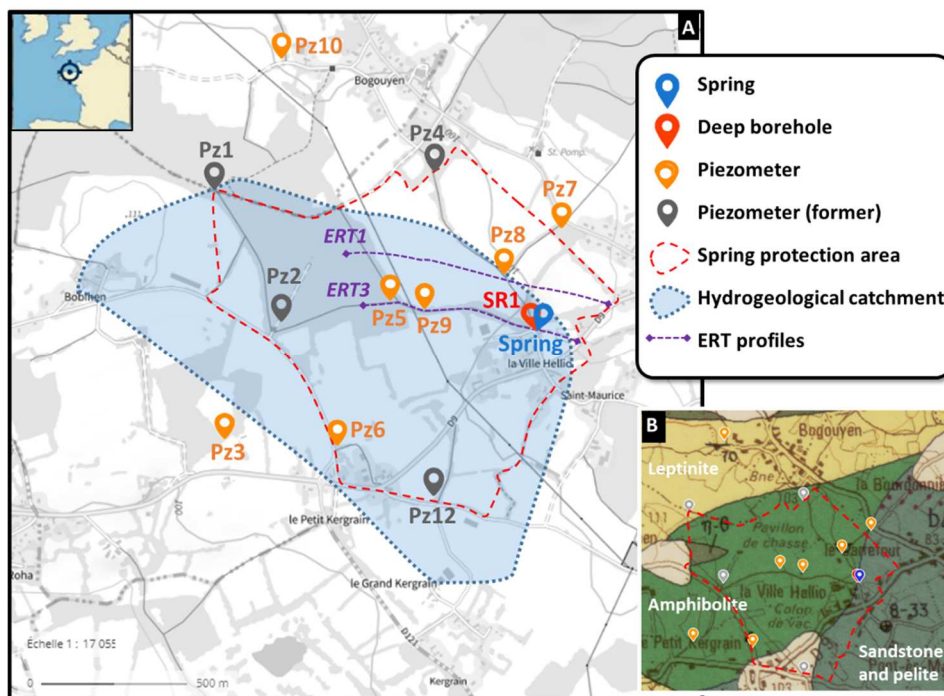
120 The Plourhan site we studied is a small (1.26 km<sup>2</sup>) hydrogeological catchment. In 2006, a  
121 potentiometric map was drawn for resource-protection purposes, relying on different  
122 hydrogeological approaches such as the drilling of 12 piezometers and a deep borehole. It is  
123 located 10 km from the coast in Brittany (northwest France). Geologically, it is underlain by  
124 Brioverian basement composed of metasedimentary pelite and sandstone, and amphibolite,  
125 both overlain by an 8 to 20 m thick saprolite layer. The basement that can be highly  
126 fractured, especially the amphibolite. A major fault forms the boundary between  
127 metasediments and amphibolite, with a potentially wide fracture zone (Figure 1). This  
128 description, based on the 1:50,000-scale geological map was not precise enough in view of  
129 the small catchment size. For this reason, a detailed geological survey of the catchment was  
130 part of this study as was a geophysical survey, providing a better definition of the detailed  
131 geology and its geometry (see Supplementary material). In addition, a pedological study  
132 carried out during delineation of the area to be protected, showed relative soil uniformity of  
133 the site. The soil is brown and moderately deep (40 cm on average in the east of the site and  
134 about 80 cm in the southwest). Under the forest, to the northwest, a particular pedogenesis is  
135 observed, the soil being pseudo-gley.

136 A natural spring emerges near the major fault and has been exploited since 1968 via a 4.4 m  
137 deep borehole that taps the water coming from the saprolite layer. This spring, hereafter  
138 referred to as Spring, feeds a small stream that exits the basin to the east. In 2006, 12  
139 piezometers (Pz1 to Pz12), between 10 and 22 m depth, were drilled mainly for delineating  
140 the catchment. In these piezometers, the groundwater level is few metres below the soil level  
141 (bsl). They are screened all along the weathered layer down to the top of the “fresh”  
142 basement. The saturated zone is only a few metres thick. A few measurements before our  
143 study showed strong heterogeneity of the groundwater quality. Monthly monitored water  
144 levels between October 2006 and March 2008 were used for drawing potentiometric maps,  
145 thus defining the hydrogeological contours of the catchment and identifying flow directions  
146 (Fig. 1). Not surprisingly, the hydrological and topographic catchments have different  
147 boundaries. Thus, for the piezometers accessible during this study, Pz3, 6 and 8 are located

148 upstream (respectively south and north of the Spring), while Pz5 and Pz9 are located in the  
149 middle of the catchment. The others (Pz10 and Pz7) lie outside the catchment.

150 In addition to these 12 piezometers tapping water in the saprolite, a deep borehole (SR1),  
151 drilled at about 30 m from the natural Spring within the fault zone, has a total depth of 133 m.  
152 It is screened below 50 m (bsl) and intersected paragneiss, and metamorphic sandstone and  
153 pelite.

154 The water supply for the 2 000 inhabitants is based on the water pumped from the Spring  
155 (Figure 1) which must be diluted in order to fulfil the drinking-water quality standards for  
156 nitrate. Indeed, the Spring has nitrate concentrations exceeding the 50 mg/L drinking water  
157 standard and the dilution takes place at the treatment plant with water from another borehole.

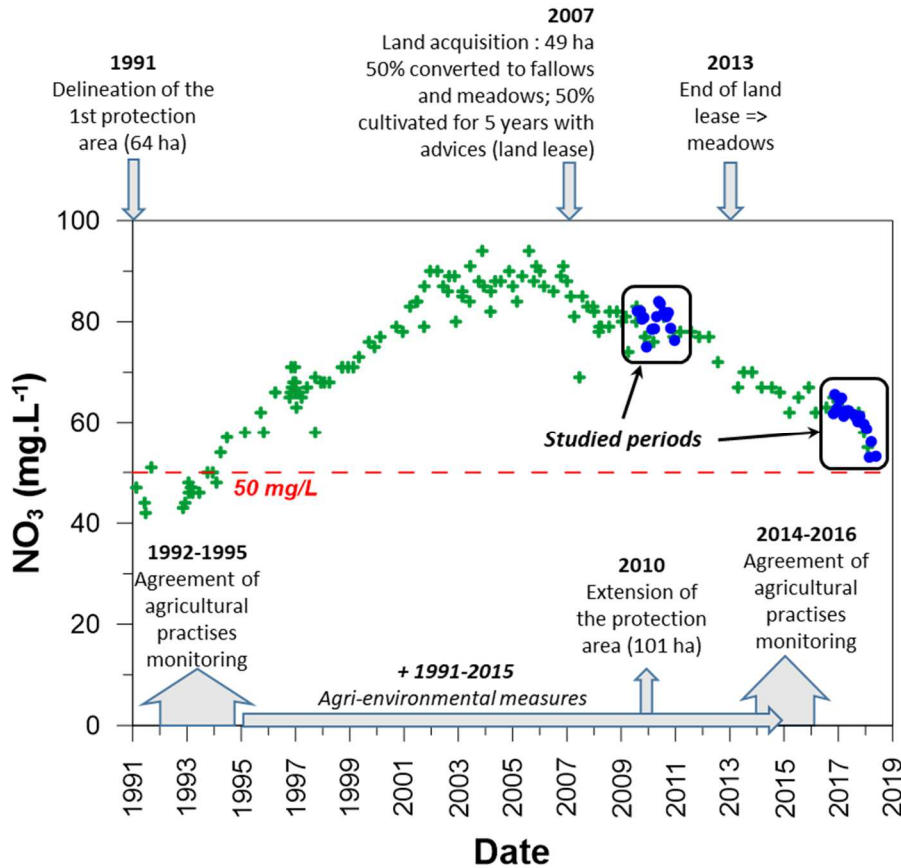


158  
159 *Figure 1: (A) Location of sampling sites and geophysical investigations in the Plourhan site (NW*  
160 *France; background 1:25,000-scale IGN map). Piezometers with grey symbols are no longer*  
161 *accessible. (B) Geological map of the studied area (@BRGM Pontrieux sheet, 1:50,000 scale).*

162 A protection area for the groundwater catchment was administratively defined in 2010 along  
163 parcel boundaries. It specified the regulation of (agricultural) land use, maintaining plots in  
164 forest or meadow areas, and plots where annual crops were allowed with specific agronomic  
165 recommendations. As of 2013, annual crops were no longer allowed and were replaced by  
166 meadows (Figure 2).

167 Historically, the studied site has been subject to strong agricultural pressure. From 1980 to  
168 1990, vegetable production dominated. In the mid-1990s, land use was mainly dedicated to  
169 market gardening, with a significant surface for peas, potatoes and cauliflower. From the

170 mid-1990s to the present, in an effort to improve groundwater quality, farmers significantly  
 171 reduced the vegetable areas (Figure 2), compensated by an increase in wheat, maize and  
 172 especially grass. Despite these efforts, nitrate concentrations in Spring water only decreased  
 173 slowly and still remain above the 50 mg/L standard (Figure 2).



174

175 *Figure 2: Temporal evolution of the nitrate concentrations in the Spring since the early 1990s (green crosses).*  
 176 *Both studied periods (2009-2011 and 2016-2018) are shown as blue dots. Historical data are from the French*  
 177 *national groundwater database (ades: <https://ades.eaufrance.fr>). History of the measures for improving water*  
 178 *quality is indicated.*

179

180 In the area, historically and until recently, nitrogen was applied in both mineral and organic  
 181 form, depending on the cultivated plot. Detailed information is not available, but it is known  
 182 that in 2014, in the protection area, four of the seven farms produced animal excrements  
 183 (cattle, pigs, poultry) and five had plots on which animal excrements, green-waste compost  
 184 and/or household waste were spread (Côtes d'Armor Chamber of Agriculture, 2014).

185 A detailed knowledge of land use allows addressing the issue of why groundwater quality is  
 186 spatially heterogeneous. Such groundwater catchment is representative of lithology  
 187 (basement), soil and climate of France and Western Europe.

188

## 189 3 Material and methods

190

### 191 3.1 Sampling strategy

192 The study site was monitored for two distinct periods. The Spring was sampled on a monthly  
193 basis from August 2009 to June 2010 (10 campaigns = 1<sup>st</sup> period) and from October 2016 to  
194 July 2019 (28 campaigns = 2<sup>nd</sup> period), whereas piezometers were only sampled twice and  
195 four times during the 1<sup>st</sup> and 2<sup>nd</sup> periods, respectively. It should be noted that some  
196 piezometers were no longer accessible during the 2<sup>nd</sup> period. Prior to sampling, several field  
197 parameters were measured, including electrical conductivity, pH, redox and oxygen content  
198 (Table S1 Supplementary material). Major ions were analysed for all samples.  
199 Microbiological parameters were measured in each samples from the 2<sup>nd</sup> period, as was  
200 groundwater dating. Isotopic investigations only concerned samples from April 2017.

201

### 202 3.2 Chemical and isotopic investigations

#### 203 3.2.1 Analytical methods

204 For both sampling periods, the groundwater samples were collected in polyethylene bottles  
205 and filtered through 0.45 µm PVDF filters for chemical and nitrate isotopes analysis. Bottles  
206 dedicated to cation analysis were acidified with 15N ultrapure HNO<sub>3</sub> to pH<2.  
207 Physicochemical parameters of each sample were measured on site, including the electrical  
208 conductivity (EC), standardized to 25 °C, water temperature, pH, dissolved oxygen (O<sub>2</sub> diss.)  
209 and redox potential (Eh). Samples were stored at 4 °C in the dark prior to analysis; this took  
210 place in the BRGM Laboratories by ICP-AES (Ca, Na, K, Mg; uncertainty <10%), ion  
211 chromatography (Cl, SO<sub>4</sub>, NO<sub>3</sub>, uncertainty <10%) and titration method according to N EN  
212 ISO 9963-1(HCO<sub>3</sub><sup>-</sup>; CO<sub>3</sub><sup>2-</sup>, uncertainty <5%).

213 Both δ<sup>15</sup>N and δ<sup>18</sup>O of NO<sub>3</sub> were measured by the AgNO<sub>3</sub> method at BRGM according to the  
214 following procedure: The filtered water is chemically purified through cationic and anionic ion-  
215 exchange columns. Nitrate is recovered as HNO<sub>3</sub> by HCl elution. The eluate is converted to  
216 AgNO<sub>3</sub> by addition of silver oxide (Ag<sub>2</sub>O): HCl + HNO<sub>3</sub> + Ag<sub>2</sub>O => AgCl<sub>(s)</sub> + AgNO<sub>3</sub> + H<sub>2</sub>O.  
217 The filtrate containing the nitrate, once freed from the other oxygenated compounds by  
218 adding BaCl<sub>2</sub>, is lyophilized to obtain solid AgNO<sub>3</sub> (Chang et al., 1999, Silva et al., 2000). The  
219 solid AgNO<sub>3</sub> precipitate is then weighed into silver capsules that are inserted separately into  
220 a furnace composed of a glassy carbon reactor heated to 1450 °C. The N<sub>2</sub> and CO gases  
221 resulting from high-temperature combustion are driven by a helium flow to a chromatographic  
222 column. This separates the gas peaks before their introduction into the source of the mass  
223 spectrometer for determining the nitrate δ<sup>18</sup>O and δ<sup>15</sup>N isotopic ratios. The analytical  
224 accuracy is ± 0.5 ‰ for δ<sup>15</sup>N and δ<sup>18</sup>O.

225 Water samples for chlorofluorocarbons and sulphur hexafluoride (CFCs and SF<sub>6</sub>) analyses  
226 were collected in stainless-steel ampoules (40 mL and 300 mL, respectively) after rinsing  
227 them with at least three times the sample volume, without any contact with atmospheric air  
228 during sampling. The CFCs and SF<sub>6</sub> concentrations, used for calculating of groundwater  
229 residence times, were measured using a gas chromatograph with an electron capture  
230 detector (GC-ECD) (Labasque et al., 2006; Ayraud et al., 2008), at the Plateforme  
231 CONDATE Eau (OSUR, University of Rennes 1, France) for the 2<sup>nd</sup> period. The  
232 concentrations of CFC-11, CFC-12 and CFC-113 were measured with an analytical  
233 uncertainty of 1%, and the SF<sub>6</sub> with an uncertainty of 5% (Labasque et al., 2006; Ayraud et  
234 al., 2008). Gas concentrations were used for calculating atmospheric mixing ratios (pptv),  
235 and compared to the atmospheric evolution curve (NOAA HATS program), to determine the  
236 apparent groundwater piston age. For each sampling point, three hypothetical lump  
237 parametric models, a piston-flow model (PFM), an exponential model (EM), and a binary  
238 mixing model (BMM), were systematically tested to determine the apparent groundwater  
239 residence time (Matoszewski and Zuber, 1996). The overall uncertainty of derived  
240 groundwater-age estimates, including sampling biases and analytical errors, as well as the  
241 errors resulting from uncertainty of the recharge temperature and considering dispersion-  
242 adsorption effects, is estimated to be ±3 years (Labasque et al., 2014). For the first sampling  
243 period (2009-2011) a simplified sample collection method was used (IAEA, 2006). The  
244 analyses were made by Spurenstofflabor at Wachenheim (Germany), using gas  
245 chromatography with an electron-capture detector after pre-concentration using the purge-  
246 and-trap technique. The detection limit was 10<sup>-4</sup> pmol, allowing the measurement of CFC  
247 concentrations down to 0.01 pmol.L<sup>-1</sup> and of SF<sub>6</sub> concentrations to 0.1 fmol. L<sup>-1</sup>;  
248 reproducibility was about ± 5% for water samples.

249 Major and noble gases were measured throughout the sampling campaign using a GC-TCD  
250 (CG 3000, SRA instrument) after headspace extraction with a He gas phase following the  
251 Sugisaki and Taki method (1987). The analytical error for Ne and Ar/N<sub>2</sub> measurements was  
252 3% and 2%, respectively. The analysis of Ne/Ar ratios allows calculating excess air and  
253 recharge temperatures (Heaton and Vogel, 1981).

### 254 3.2.2 N and O isotopes of nitrate theoretical background

255 Since the 2000s, nitrogen and oxygen isotopes of nitrates ( $\delta^{15}\text{N-NO}_3$  and  $\delta^{18}\text{O-NO}_3$ ) are used  
256 for tracing nitrate sources in surface and groundwaters (Widory et al., 2005, 2013; Kendall et  
257 al., 2007; Fenech et al., 2012; Puig et al., 2017). Nevertheless, N-sources discrimination is  
258 often not straightforward as nitrate is not a conservative molecule, and thus the N  
259 transformation process has to be considered for properly tracing N sources. N and O  
260 isotopes are also valuable tracers for better constraining the N cycle from soil to

261 groundwater, i.e. immobilization, mineralization, nitrification and denitrification. These  
262 different processes may thus lead to a loss of the original  $\delta^{15}\text{N-NO}_3$  and  $\delta^{18}\text{O-NO}_3$  isotopic  
263 signatures through isotopic fractionation (Zhang et al., 2019). However, such isotopic  
264 fractionations is an excellent tool for identifying these processes and thus for better  
265 constraining N mobility.

266 Denitrification by oxidation of pyrite ( $\text{FeS}_2$ ), i.e. during chemoautotrophic respiration of  
267 sulphur-oxidizing *Thiobacillus denitrificans*, has been identified as an important denitrification  
268 pathway in basement aquifers where pyrite is abundant (Pauwels et al., 2000). Note that  
269 Aquilina et al. (2018) suggested another type of autotrophic denitrification: biotite dissolution  
270 with the oxidation of Fe(II) contained in biotite. Denitrification is a highly fractionating process  
271 (Böttcher et al., 1990; Kendall and Aravena, 2000), following a Rayleigh distillation model,  
272 leading to a joint increase of the isotope ratios  $\delta^{15}\text{N-NO}_3$  and  $\delta^{18}\text{O-NO}_3$  of the residual  $\text{NO}_3$ .  
273 The N cycle in soil further modifies the isotopic signature of the nitrate leached out and  
274 transported toward groundwater (Mengis et al., 2001, Sebilo et al., 2013). The newly formed  
275 nitrate through ammonium nitrification is generally assumed to take nitrogen from  $\text{NH}_4^+$   
276 (and/or  $\text{NO}_2$ ), while one oxygen comes from atmospheric  $\text{O}_2$  and two from water ( $\text{H}_2\text{O}$ )  
277 considering a simple stoichiometric relationship (Equation 1; Kumar et al., 1983; Kendall,  
278 1998 and references therein); Note that Buchwald and Casciotti (2010) added constraints to  
279 this simple model considering oxygen isotope exchanges of intermediate species with  
280 ambient water, during nitrite oxidation corresponding to the final step of nitrification process.

281 
$$\delta^{18}\text{O-NO}_3 = \frac{2}{3} (\delta^{18}\text{O-H}_2\text{O}) + \frac{1}{3} (\delta^{18}\text{O-O}_2) \quad (\text{Equation 1})$$

282

### 283 3.3 Microbiological and biomolecular approaches.

284 The spatial and temporal evolution of the abundance of bacteria involved in nitrate reduction  
285 was assessed through measurements of nitrate reductase encoding genes *narG* and *napA*  
286 copies. In November 2016, April and October 2017, and May 2018, water (6 L) was collected  
287 from each piezometer and filtered (0.22  $\mu\text{m}$ ) to collect biomass. Microbial DNA was extracted  
288 from the filters using a FastDNA™ Spin Kit for Soil (MP Biomedicals, USA) according to  
289 manufacturer's recommendations, with a FastPrep®-24 at a speed of 5  $\text{m.s}^{-1}$  during 30 s,  
290 and quantified with a Quantifluor dsDNA sample kit and the Quantus fluorimeter, according  
291 to the manufacturer's instructions (Promega, USA). The abundances of *narG* and *napA* gene  
292 copies was determined by real-time quantitative PCR (qPCR) according to Bru et al. (2007).

293

294 In order to assess potential denitrification activity, batch experiments were run on waters  
295 sampled in April 2017 in the Pz3, Pz6, Pz8, Pz9 and Pz10 piezometers. Briefly, duplicate

296 300 mL flasks were filled in with 150 mL of water under anaerobic conditions (nitrogen  
297 atmosphere). Acetate ( $C_2H_3NaO_2$ ) was added as a carbon source in each flask at a final  
298 concentration of 100 mg/L. Considering nitrate concentration in each well, nitrate was added  
299 to the flasks to reach a final  $NO_3^-$  concentration of 100 mg/L. Abiotic tests in the presence of  
300 sodium azide (Cabrol *et al.*, 2017) were also performed. The flasks were incubated for 20  
301 days in the dark at 25 °C under stirring (100 rpm). Every 4 to 5 days, 8 mL of water was  
302 sampled for nitrate, nitrite and acetate quantification, and 5 mL of the gas phase was  
303 sampled for  $N_2O$  analysis. Nitrate and acetate were quantified by ionic chromatography  
304 (Dionex IC3000-SP-EG-DC system equipped with an AS50 autosampler and a  
305 conductimetric detector) according to the NF EN ISO 10304-1 (2009) method. Nitrite was  
306 analysed by colorimetry according to the NF ISO 15923-1 (2014) method.  $N_2O$  was analysed  
307 by gas chromatography (Varian CP-3800 GC equipped with a gas injection valve and an  
308 electron capture detector).  
309 For statistical analysis, boxplots were calculated using R4.0.1 and RStudio (n=2). Data were  
310 analysed by the non-parametric Kruskal-Wallis test ( $p>0.05$ ).

311

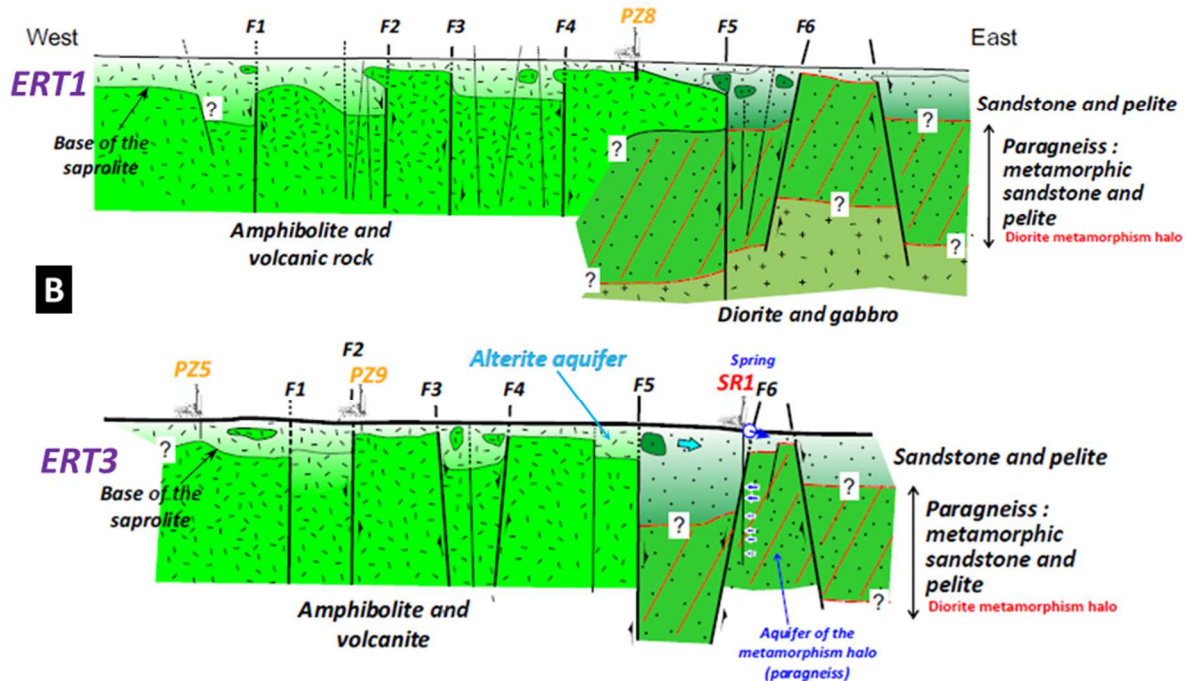
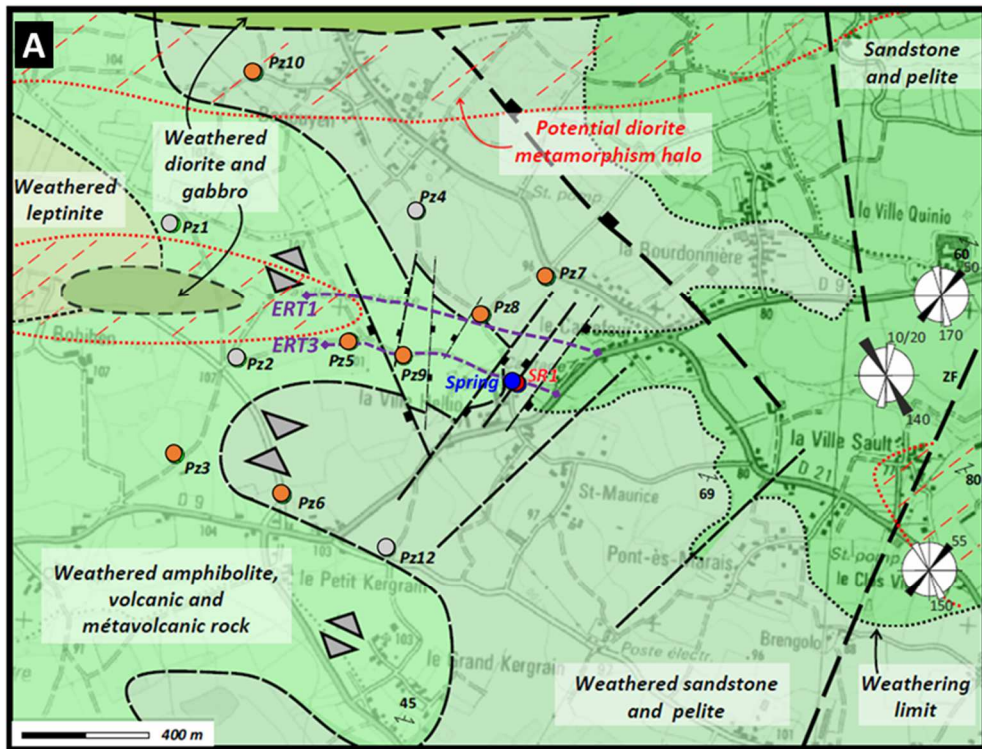
## 312 **4 Results and discussions**

313

### 314 **4.1 Improving of the hydrogeological model**

315 Geological investigations consisted in accurately identifying the rock types, tectonic  
316 structures and degree of weathering, in order to refine the geological map at the scale of this  
317 small catchment and to better understand the hydrogeological functioning. This field work  
318 confirmed that the catchment is located on a Brioverian anticlinal axis oriented N100/110,  
319 intersected by faults oriented N150, sub N-S and N050. The weathering profile forms a  
320 paleosurface at an altitude of about 80 m above mean sealevel, and seems to be affected  
321 by faulting.

322



323

324

325

Figure 3: (A) Revised geological map of the study area. (B) Geological cross-sections derived from the electrical resistivity distribution profiles (FIG S1 in supplementary material).

326

327

328

329

330

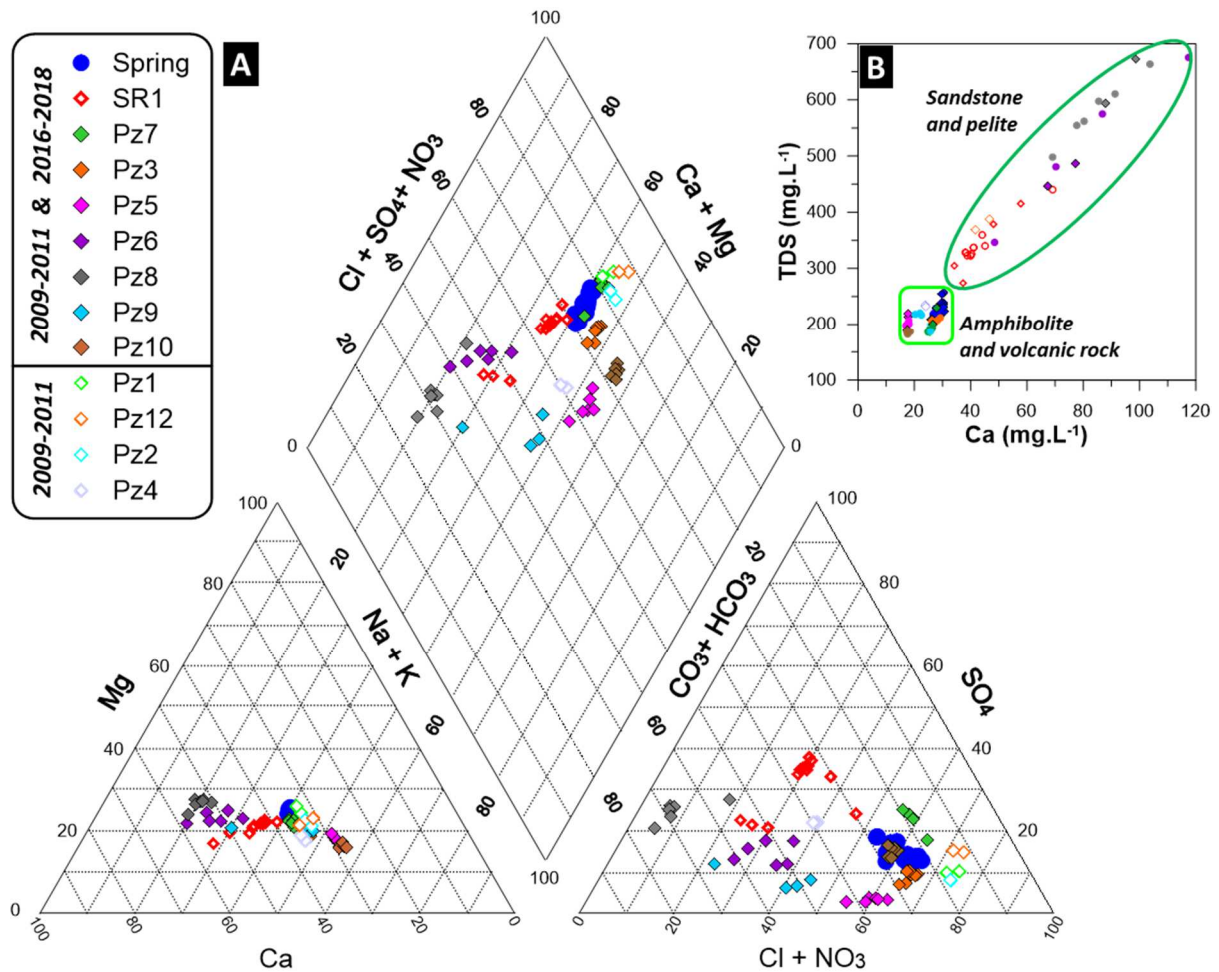
331

Geophysical results showed major horizontal resistivity contrasts, with two distinct domains separated by a significant vertical discontinuity (F5; FIG. S1 Supplementary material). The western resistive domain corresponds to amphibolite, while the conductive eastern unit corresponds to metamorphic sandstone and pelite (Egal et al., 1996; Figures 1 and 3A). To the west, a vertical resistivity gradient is interpreted as a signature of the amphibolite weathering profile consisting of alterite (C0, Fig. S1) at the top, followed by a fractured layer

332 (R1) and fresh basement rock (R2). These results are coherent with those observed in other  
333 basement contexts (Dewandel et al., 2006; Belle et al., 2019; Comte et al., 2012;). In the  
334 sandstone and pelite domain, despite the complexity of the electrical pattern, the SR1  
335 geological log distinguishes the alterite from the sandstone and pelite (C1, C2, Fig. S1) that  
336 overlie a highly conductive C3 paragneiss derived from the sandstone and pelite, forming a  
337 metamorphic halo (Egal et al., 1995) and being an aquifer formation. This suggests that the  
338 high conductivity values observed are caused by strong and connected fracturing of the rock,  
339 and thus that the paragneiss is the main aquifer formation of the catchment. The amphibolite  
340 seems more impermeable than the sandstone and pelite, and the alterite forms a surface  
341 aquifer (Figure 3). Further details are presented in the Supplementary material.

342 To complete the geological and geophysical investigations and improve preliminary  
343 conclusions, chemical data were examined (Figure 4). The total mineralization of the water  
344 can be assessed through its electrical conductivity (EC,  $\mu\text{S}\cdot\text{cm}^{-1}$ ) and the Total Dissolved  
345 Solids (TDS,  $\text{mg}\cdot\text{L}^{-1}$ ), both parameters being correlated. The TDS values of the Spring  
346 samples (natural outlet of the hydrogeological system) show small variations over the two  
347 sampling periods (205-257  $\text{mg}\cdot\text{L}^{-1}$ ), as do most groundwater samples within the catchment  
348 (182-235  $\text{mg}\cdot\text{L}^{-1}$ , Pz1, Pz2, Pz3, Pz4, Pz7, Pz9 and Pz10). Nevertheless, four groundwater  
349 samples (Pz6, Pz8, Pz12 and SR1) have clearly higher TDS values, ranging between 274  
350 and 675  $\text{mg}\cdot\text{L}^{-1}$ , varying both throughout the sampling periods and according to the sampling  
351 depth (Figure 4B). Groundwater presents very heterogeneous chemical types at this small  
352 catchment scale, from Ca-HCO<sub>3</sub> to Ca-SO<sub>4</sub>. Cation proportions vary between a sodic end-  
353 member (>50% Na+K, in Pz10) and a calcic end-member (up to 60% Ca), in Pz6 and Pz8  
354 (Figure 4A).

355



356

357 *Figure 4 : (A) Piper diagram of the Plourhan groundwater samples. Both studied periods are shown, empty*  
 358 *symbols are samples with data only available during the first period 2009-2011. (B) Total Dissolved Solids (TDS)*  
 359 *versus Ca concentration.*

360 When comparing the revised structural scheme (Figure 3) and the geochemical data, it  
 361 appears that samples with the higher calcium concentrations (i.e. Pz6, Pz8, Pz12 and SR1),  
 362 which also have the highest TDS, reflect water-rock interactions with the weathered  
 363 sandstone and pelite compartment. The other samples with low TDS values and lower  
 364 calcium concentrations seems to results from water-rock interaction with the weathered  
 365 amphibolite compartment. This chemical variability also reflects the complex geological  
 366 settings of this small area (only 0.6 km<sup>2</sup>), in terms of both weathering profile and geological  
 367 entities.

368 It is worth noting that water in the deep borehole SR1 has an increasing Ca load with depth,  
 369 probably related to water rock-interaction with fractured sandstone. In addition, Pz4 and Pz7  
 370 in the weathered sandstone and pelite compartment, present geochemical signatures very  
 371 similar to that of groundwater in the amphibolite compartment. The geological and  
 372 geophysical investigations allowed refining the contours of each geological formation on the  
 373 1:50,000-scale geological map, these contours being coherent with the geochemical

374 groundwater signatures. However, interrogations remain for some piezometers that are too  
375 far from the two geophysical profiles for making sufficiently reliable projections.

376

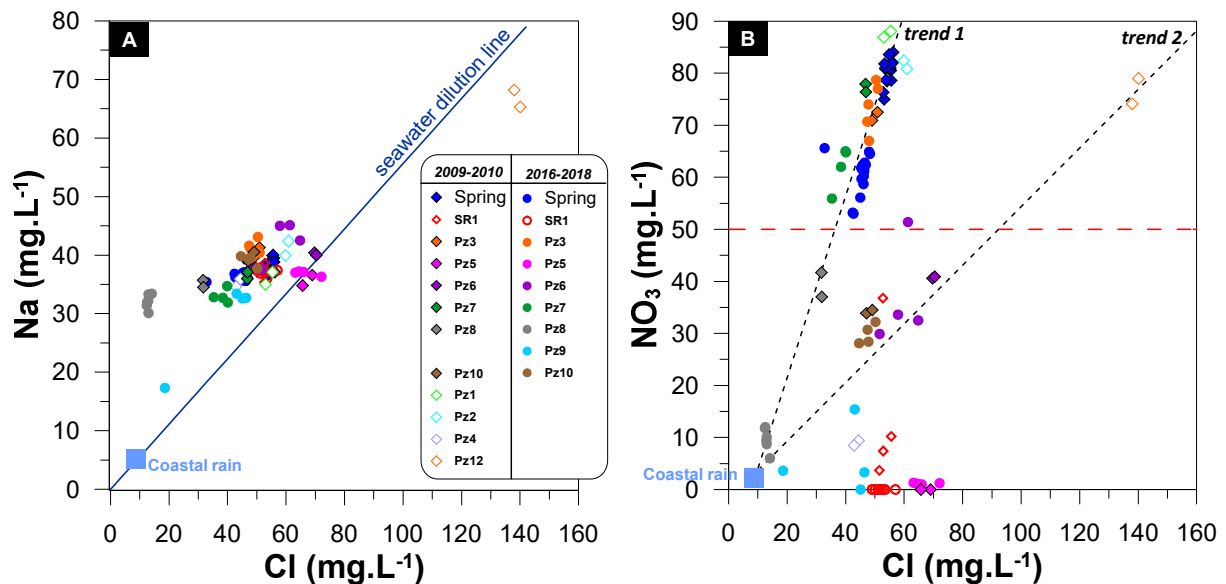
#### 377 4.2 Temporal and spatial anthropogenic pressure: a focus on nitrate

378 As mentioned above, despite all efforts made to reduce nitrogen transfer to groundwater,  
379 nitrate concentrations only decrease slowly at the Spring and remain above the 50 mg.L<sup>-1</sup>  
380 standard (Figure 2). The increase in NO<sub>3</sub> concentrations has stopped in the early 2000s,  
381 reaching a plateau over five years before starting a decrease that continues today. This type  
382 of evolution is typical of what is commonly observed in Europe since the implementation of  
383 various programmes of measures for recovering a good chemical status of the groundwater  
384 bodies, even though the response time can be quite different (European Commission, 2018).

385 This anthropogenic pressure is clearly shown in the small Plourhan catchment, where nitrate  
386 concentrations in groundwater can be as high as 88 mg.L<sup>-1</sup> (Pz1, Oct-2009). However, the  
387 nitrate concentrations in the piezometers sampled during the two sampling periods (2009-  
388 2010 and 2016-2018), showed quite different values from one piezometer to the next. For  
389 instance, the Spring and PZ7 showed a NO<sub>3</sub> decrease between the 1<sup>st</sup> and 2<sup>nd</sup> periods, from  
390 80 to 61 mg.L<sup>-1</sup> (Spring) and from 77 to 62 mg.L<sup>-1</sup> (Pz7) (Figure 2; Figure 5B; table S1  
391 Supplementary material). Pz8 has the largest decrease in nitrate concentrations, from 39 to  
392 10 mg.L<sup>-1</sup> on average between the two sampling periods. The temporal variations between  
393 1<sup>st</sup> and 2<sup>nd</sup> periods are less pronounced for Pz3 and Pz6. Most of the groundwater samples  
394 from piezometers PZ5 and Pz9, and borehole SR1 now have nitrate concentrations below 10  
395 mg.L<sup>-1</sup>.

396 Figure 5A shows the sodium *versus* chloride concentrations in groundwater of the study  
397 area. In the absence of evaporites in the local geological formations, chloride may derive  
398 from atmospheric (Meybeck, 1983) or anthropogenic (agriculture, wastewater effluents, etc.)  
399 inputs and thus may have the same origin as nitrate. Significant amounts of chloride (> 80  
400 mg.L<sup>-1</sup>) were measured in many groundwaters of the Brittany basement (> 80m deep) that  
401 were shown to be related to the last marine Mio-Pliocene transgressions, while shallow and  
402 modern groundwater has lower Cl concentrations (< 50 mg.L<sup>-1</sup>) (Aquilina et al., 2015). In this  
403 study, groundwater samples were taken at 10 to 22 m depth in the weathered layer and at  
404 the top of the basement, except in the SR1 borehole that is 133 m deep. The Cl  
405 concentrations are generally less than 60 mg.L<sup>-1</sup> including in borehole SR1. Only Pz12  
406 presents a clearly higher Cl concentration of ~140 mg.L<sup>-1</sup> (two samples in 2009), as does Pz5  
407 with Cl concentrations of 72 mg.L<sup>-1</sup> (the specific case of Pz5 is further discussed in section  
408 4.3). For most groundwater samples, Figure 5A shows an excess of sodium relative to the

409 Na/Cl marine ratio, reflecting Na release in solution through interaction of groundwater with  
 410 silicate minerals of the aquifer matrix. Only Pz12 has an excess of chloride compared to the  
 411 Na/Cl ratio of the seawater dilution line, which may indicate anthropogenic input of Cl (both  
 412 Na and Cl concentrations being higher than in the other samples). Manure and sewage  
 413 effluents are known to be rich in Cl (Kloppmann, 2003), and KCl is used as fertilizers or road  
 414 salts. The  $\text{NO}_3/\text{Cl}$  ratios of manure and sewage are generally lower than in mineral fertilizers,  
 415 and can thus help distinguishing various anthropogenic sources (Lu et al., 2015). Moreover,  
 416 the  $\text{NO}_3/\text{Cl}$  ratio may indicate a dilution effect *versus* nitrate removal through denitrification,  
 417 as Cl behaves conservatively (Chen et al., 2009, Widory et al., 2013). Figure 5B shows  $\text{NO}_3$   
 418 vs. Cl concentrations, part of the groundwater samples with the highest nitrate  
 419 concentrations (Spring, Pz7, Pz3, Pz2 and Pz1) defining a straight line correlating  $\text{NO}_3$  and  
 420 Cl concentrations (*trend 1*, Figure 5B), suggesting a common origin of both elements, i.e.  
 421 that at least part of the Cl is anthropogenic. For the Spring and Pz7 that were sampled during  
 422 both sampling campaigns,  $\text{NO}_3$  and Cl concentrations decrease jointly between the two  
 423 sampling periods, confirming this hypothesis. Pz12 with high  $\text{NO}_3$  concentrations (75-80  
 424  $\text{mg.L}^{-1}$ ) has a different  $\text{NO}_3/\text{Cl}$  ratio, with a higher Cl proportion. This may reflect a different  
 425 anthropogenic source with a lower  $\text{NO}_3/\text{Cl}$  than previous samples, which could be related to  
 426 manure input (*trend 2*, Figure 5B). Note that, as Pz12 is no longer accessible; it was not  
 427 possible to resample this well during the 2<sup>nd</sup> period.



428  
 429 *Figure 5 : (A) Sodium versus chloride concentrations in Plourhan groundwater samples. 'Coastal rain' refers to*  
 430 *the mean rainfall at Brest (100 km to the west; Negrel et al., 2007). The Seawater dilution line (Bernier-Kay and*  
 431 *Bernier, 1987) is presented as reference. Both studied periods are plotted, each sampling point has the same*  
 432 *colour with different symbols: empty ones are samples from the first period (2009-2010). (B) Nitrate versus*  
 433 *Chloride concentrations in Plourhan groundwater. The red dashed line represents the 50 mg.L<sup>-1</sup> nitrate standard.*  
 434 *The black dashed lines represent the two main NO<sub>3</sub> vs. Cl trends.*

435 **Figure 5B** also shows groundwater samples that clearly differ from the previous group, with  
436 similar Cl but lower NO<sub>3</sub> concentrations. Two sub-groups occur: a first one with NO<sub>3</sub> < 20  
437 mg.L<sup>-1</sup> and Cl > 40 mg.L<sup>-1</sup> (Pz4, Pz5, Pz9, SR1), which may result from nitrate loss through  
438 denitrification, or even no nitrate input. Note that Cl concentrations are in the range 40-75  
439 mg.L<sup>-1</sup>, except Pz9 sampled in April 2017 with 18 mg.L<sup>-1</sup>. The second sub-group shows  
440 intermediate nitrate concentrations (~30-50 mg.L<sup>-1</sup> in Pz6 and Pz10, and one SR1 sample at  
441 60 m depth in November 2009), together with Cl ranging from 40 to 75 mg.L<sup>-1</sup>. Such  
442 characteristics may result from two distinct scenarios: (1) partial denitrification in water with  
443 similar Cl and higher NO<sub>3</sub> concentrations (i.e. similar to the Spring signature); or (2) mixing  
444 between a groundwater component with an anthropogenic impact similar to that described  
445 for Pz12, and a groundwater component with low NO<sub>3</sub> and low Cl, typical of recharge by  
446 rainwater. Finally, the Pz8 groundwater samples have NO<sub>3</sub> and Cl concentrations that  
447 strongly decreased between the two sampling periods, in the same proportions that were  
448 observed for the Spring group. Moreover, the 2018 samples, which have similar Cl  
449 concentrations, have NO<sub>3</sub> concentrations that decrease with the sampling depth, reflecting a  
450 stratification of the local groundwater.

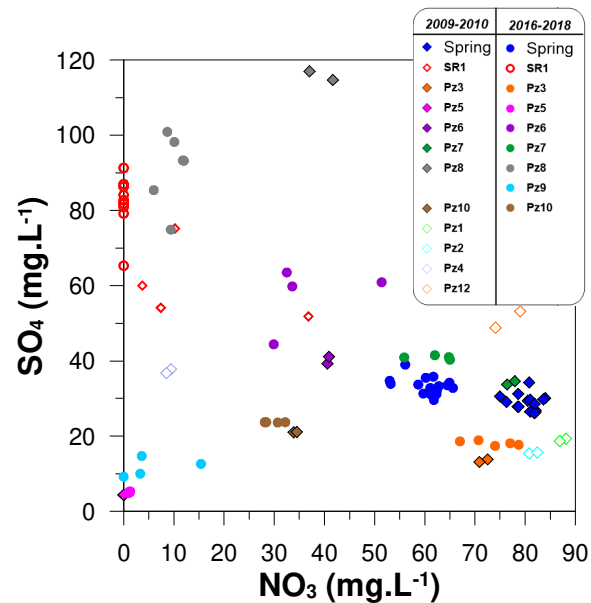
451 To summarize, the joint decrease of NO<sub>3</sub> and Cl concentrations between the two sampling  
452 periods could result from a positive impact of the mitigation measures applied on the  
453 catchment since about two decades, while a net decrease of nitrate alone should result from  
454 a chemical/microbiological process like denitrification.

455

#### 456 4.3 Evidence of denitrification processes based on N and O isotopes of 457 NO<sub>3</sub>, microbiology and molecular approaches

458 Denitrification leads to a decrease, or even 'disappearance' (below the analytical  
459 quantification limit), of nitrate concentrations in groundwater. Denitrification by oxidation of  
460 pyrite has been identified as an important denitrification pathway in the Brittany basement-  
461 rock aquifers, where pyrite is abundant (Pauwels et al., 2000). Pyrite oxidation releases  
462 dissolved sulphate in solution. Except for samples Pz5 and Pz9, discussed later, **Figure 6**  
463 shows an overall trend of increasing sulphate content when the nitrate content decreases,  
464 which is typically the case for SR1 samples; Pz8 samples were sampled at various depths  
465 and, over both sampling periods, they had the highest SO<sub>4</sub> concentrations and medium to  
466 low NO<sub>3</sub> concentrations. Even Pz6 samples could indicate denitrification through pyrite  
467 oxidation. Note that pyrite was observed in fractures of the sandstone and pelite during  
468 drilling of Pz6 and Pz8. In the Spring and Pz7 samples, while nitrate concentrations dropped

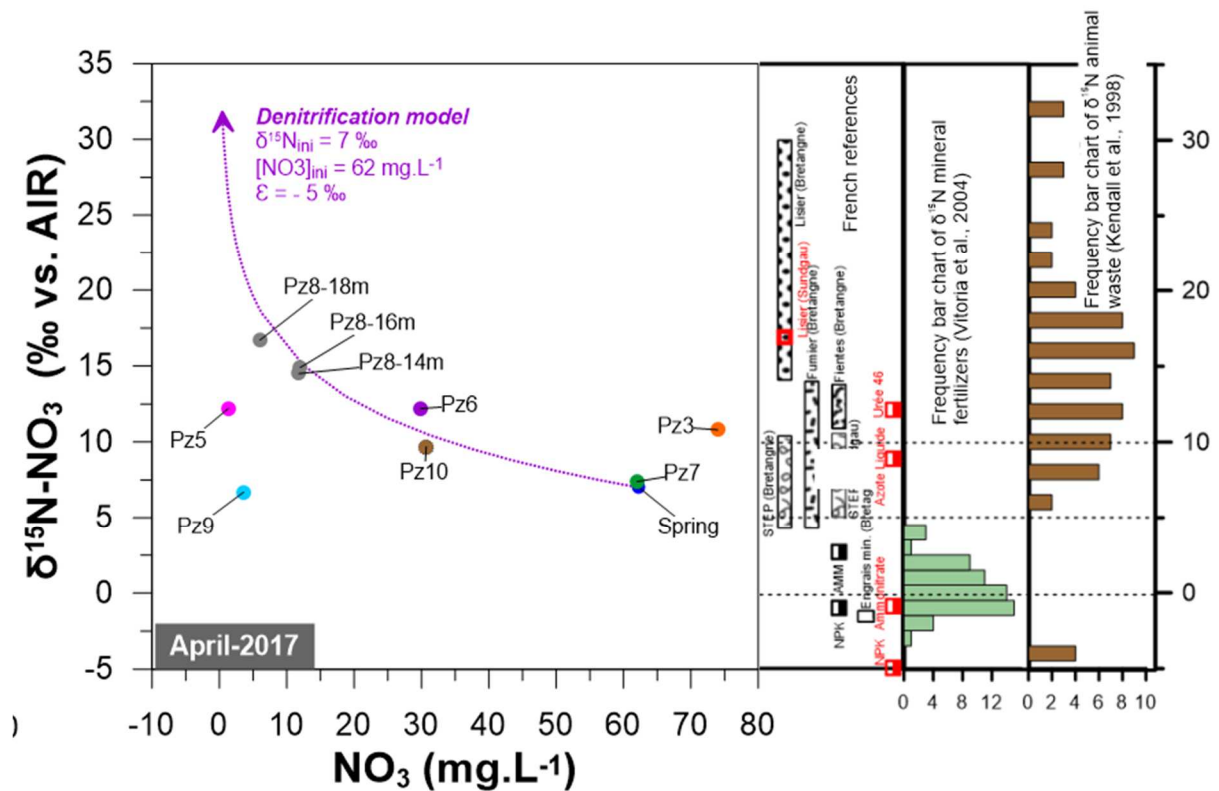
469 significantly between the two sampling periods, there was no significant increase in sulphate  
470 contents.



471

472 *Figure 6 : Sulphate versus nitrate concentrations in mg.L<sup>-1</sup> in Plourhan groundwater samples for both sampling*  
473 *periods.*

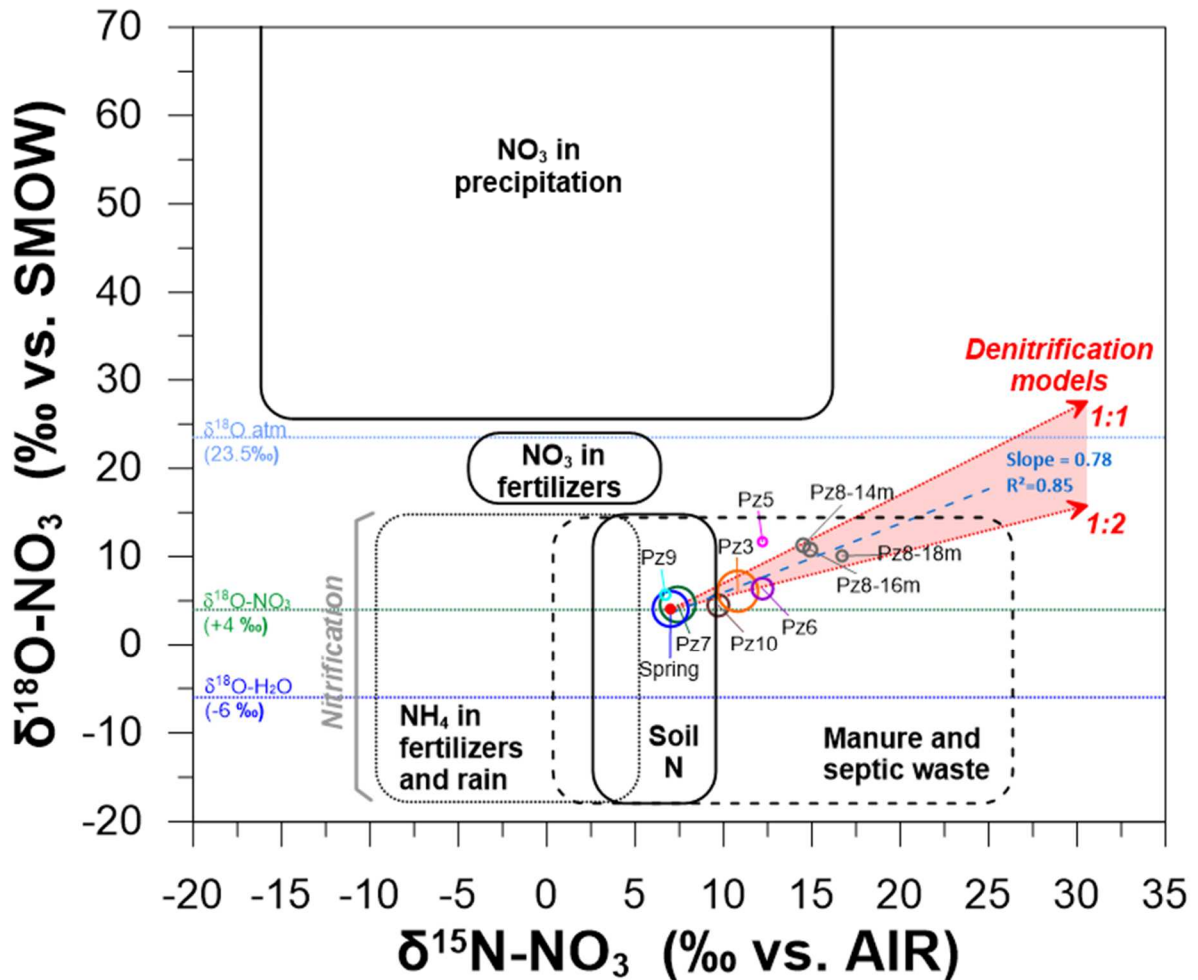
474 The dual approach of N and O isotopes of nitrate was applied to a selection of samples from  
475 each major group defined above (Figure 5B). Among these samples from April 2017, ten  
476 were analysed to determine their NO<sub>3</sub> isotopic compositions (Table S2, Supplementary  
477 material). Note that the three samples from borehole SR1 could not be isotopically analysed  
478 because nitrate concentrations were below the quantification limit. The  $\delta^{15}\text{N-NO}_3$  isotopic  
479 ratios of all samples ranged from +7 to +17‰, with nitrate concentrations ranging from 1 to  
480 74 mg.L<sup>-1</sup> in Pz5 and Pz3, respectively. For the samples with the highest nitrate  
481 concentrations, the Spring and Pz7 had a  $\delta^{15}\text{N-NO}_3$  of ~7-7.5 ‰ that could reflect a mixed  
482 influence of mineral and organic fertilizers, while Pz3 with a  $\delta^{15}\text{N-NO}_3$  of ~10.8 ‰ appears to  
483 be more influenced by organic fertilizer nitrate input (Figure 7), both types of fertilizer being  
484 used in the catchment.  
485



486

487 *Figure 7 :  $\delta^{15}\text{N-NO}_3$  vs.  $\text{NO}_3$  concentrations for the April 2017 samples. The purple dashed line represents the*  
 488 *denitrification model according to the Raleigh equation, starting from the Spring sample characteristics. Bar charts*  
 489 *on the right side represent the  $\delta^{15}\text{N}$  frequencies of mineral fertilizers and animal waste. The main nitrate sources*  
 490 *measured in France are also shown (Kloppmann et al., 2003; Widory et al., 2005).*

491 **Figure 7** also shows that, with the exception of Pz5 and Pz9, the samples present an  
 492 increasing  $\delta^{15}\text{N-NO}_3$  when  $\text{NO}_3$  concentrations decrease, which is a typical trend of  
 493 denitrification according to the Rayleigh model. Here, we chose to apply a denitrification  
 494 model starting from the sample signatures with the highest nitrate concentration, and  
 495 assumed not to be impacted by denitrification as shown by their chemical composition. The  
 496 denitrification model is thus based on the signature of Spring and Pz7 samples ( $\delta^{15}\text{N-NO}_3 = -$   
 497  $7\text{‰}$ ,  $[\text{NO}_3] = 62 \text{ mg.L}^{-1}$ ) with an enrichment factor  $\epsilon = -5\text{‰}$ . It explains a partial denitrification  
 498 for samples Pz6, Pz10 and Pz8 at different depths as these samples plot along the  
 499 calculated denitrification curve (Figure 7). The relatively low  $\epsilon$  value ( $-5\text{‰}$ ) is similar to the  
 500 one found by Pauwels et al. (2000) in the deep aquifer of the pyrite-bearing Brioverian schist  
 501 at the Naizin site (SE Brittany), and suggests a relatively rapid denitrification process  
 502 (Mariotti et al., 1988) in full agreement with the results of Pauwels et al (1998) in the same  
 503 area. Note that a low  $\epsilon$  value ( $-4\text{‰}$ ) was further confirmed in the same site during an artificial  
 504 tracer test along a fracture in the pyrite-bearing Brioverian schist basement (Petelet-Giraud  
 505 et al., 2017).



506

507 *Figure 8:  $\delta^{18}\text{O}-\text{NO}_3$  versus  $\delta^{15}\text{N}-\text{NO}_3$  with typical  $\delta^{15}\text{N}$  and  $\delta^{18}\text{O}$  values of nitrates derived or nitrified from various*  
 508 *nitrogen sources (after Kendall, 1998). The two red "denitrification" arrows indicate typical slopes expected for*  
 509 *data resulting from nitrate denitrification with initial  $\delta^{15}\text{N} = +7\text{‰}$  and  $\delta^{18}\text{O} = +4\text{‰}$ . Typical ranges of values for*  
 510  *$\delta^{18}\text{O}-\text{NO}_3$  produced by nitrification of ammonium and organic matter are referred to as "Nitrification". The size of*  
 511 *the circles for each sample of April 2017 is proportional to the measured nitrate concentration.*

512 All isotopic data of the April 2017 sampling campaign are shown in [Figure 8](#), coupling  $\delta^{15}\text{N}-$   
 513  $\text{NO}_3$  and  $\delta^{18}\text{O}-\text{NO}_3$ . Firstly, it should be noted that the original  $\delta^{18}\text{O}-\text{NO}_3$  isotope signature of  
 514 synthetic mineral fertilizers ( $\delta^{18}\text{O}-\text{NO}_3 \sim +20\text{‰}$ ) is not found in groundwater samples, even  
 515 before any denitrification (Spring and Pz7 samples). The initial  $^{18}\text{O}$  isotopic signature seems  
 516 to have been lost due to immobilization and mineralization processes of nitrogen in the soil  
 517 ([Mengis et al., 2001](#), [Sebilo et al., 2013](#)). Among the three oxygen atoms, associated with  
 518 nitrogen of the newly formed  $\text{NO}_3$ , two come from local water and one from atmospheric  $\text{O}_2$   
 519 ( $\delta^{18}\text{O}-\text{O}_2 \sim +23\text{‰}$ ; [Equation 1](#)). The isotopic signature of the local groundwater can be  
 520 approximated using the mean isotopic signature of the local rainfall (weighted average of the  
 521 precipitation amounts). According to the French national map by [Millot et al. \(2010\)](#), the local  
 522 groundwater signature is estimated to be  $\delta^{18}\text{O}-\text{H}_2\text{O} = -6\text{‰}$ . According to [Equation 1](#), the  
 523 theoretical  $\delta^{18}\text{O}$  value of the newly formed nitrate in the soil is thus  $\delta^{18}\text{O}-\text{NO}_3 \sim +4\text{‰}$ , which

524 agrees with the measured values of the Spring and Pz7 samples (+4.1 and +4.6 ‰  
525 respectively, and considering an analytical accuracy of  $\pm 0.5$  ‰).

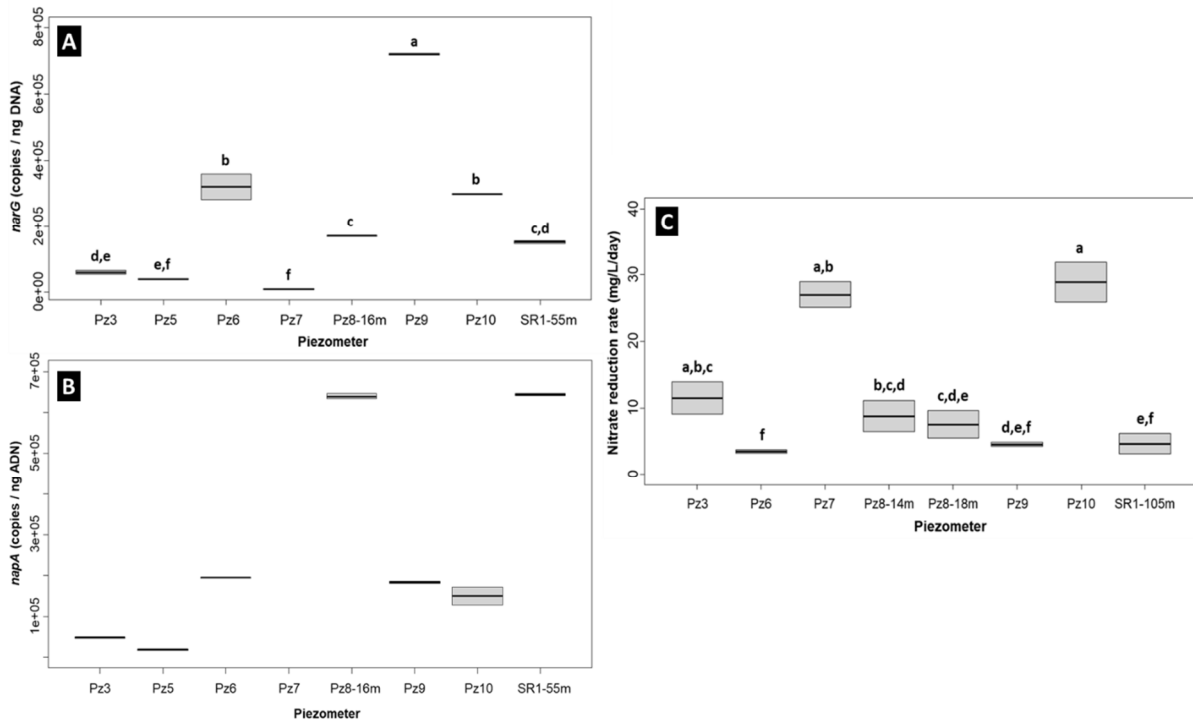
526 The dual  $\delta^{15}\text{N-NO}_3$  and  $\delta^{18}\text{O-NO}_3$  isotopic approach confirms a denitrification process for  
527 several samples, with a joint increase in the  $\delta^{15}\text{N}$  and  $\delta^{18}\text{O}$  isotopic ratios of the residual  
528 nitrate (Figure 8). The slope of the relation between  $\delta^{18}\text{O-NO}_3$  and  $\delta^{15}\text{N-NO}_3$  for the samples  
529 undergoing denitrification is 0.78 ( $R^2=0.85$ ), indicative of denitrification activity (Aravena and  
530 Robertson, 1998). In more details, samples can plot along a 0.5 slope (e.g., Pz6) and along a  
531 1 slope (e.g., Pz8-14). Compilation of a large number of environmental studies showed that  
532 denitrification increases  $\delta^{18}\text{O}$  and  $\delta^{15}\text{N}$  in a ratio of about 0.5; which corresponds to a  $^{15}\text{N}\epsilon$   
533 about twice as large as  $^{18}\text{O}\epsilon$  (Mengis et al., 1999). A lower slope between  $\delta^{18}\text{O-NO}_3$  and  $\delta^{15}\text{N-NO}_3$   
534 of nearly 0.5 was also reported from field studies, and another of nearly 1.0 from  
535 laboratory studies (Otero et al., 2009; Critchley et al., 2014; Margalef-Marti et al., 2019;  
536 Ceballos et al., 2020). The main hypothesis now recognized for this flatter slope in field-data  
537 sets compared to that in laboratory data, is the oxidation of the intermediates products ( $\text{NO}_2$   
538 and/or  $\text{NH}_4$ ) to  $\text{NO}_3$  (Granger and Wankel, 2016; Margalef-Marti et al., 2019), while a direct  
539  $\text{NO}_2$  reduction to gaseous N products might lead to values close to the theoretical 1:1 line.  
540 Thus, it is generally accepted that when isotopic nitrate data plot along a slope from 0.5 to 1,  
541 the trend can be interpreted as a denitrification process.

542 Samples Pz6, Pz10 and the three Pz8 samples (14, 16 and 18m deep) are clearly marked by  
543 a denitrification, with an alignment describing a slope between 0.5 and 1 (Figure 8). In  
544 addition, Pz6 and Pz10 samples show dissolved  $\text{N}_2\text{O}$  (intermediate denitrification product),  
545 depending on the sampling campaigns, at concentrations that can reach  $200 \mu\text{g}\cdot\text{L}^{-1}$ . It should  
546 be noted that Pz3, although in the same alignment, is not affected by denitrification, but  
547 rather by a different source of nitrate (more “organic” in this case, Figure 7 and Figure 8) with  
548 the highest  $\text{NO}_3$  concentration measured during the study. Pz5 and Pz9, with low nitrate  
549 contents (and low sulphate contents) and have  $\delta^{15}\text{N-NO}_3$  isotope signatures that do not  
550 indicate any denitrification.

551 Isotopic analyses thus suggested a microbial nitrate reduction activity in some piezometers,  
552 i.e. Pz6, Pz8 and Pz10, but not all the piezometers in the catchment. In water samples of  
553 2017, the relative abundance of copies of *narG* and *napA* genes, encoding nitrate reductases  
554 involved in nitrate reduction by denitrifying bacteria, was higher in Pz6, Pz8 and Pz10 than in  
555 other piezometers, such as Pz3, Pz5 and Pz7, for which isotopic investigation suggested no  
556 nitrate reduction (Figure 9 A and B). Results obtained from isotopic investigation and  
557 molecular analyses agree, showing higher nitrate-reductase gene abundances in  
558 piezometers where nitrate reduction was highlighted by isotopic signatures. Abundance of

559 gene copies was also assessed over a period of two years (through the four sampling  
560 campaigns including April 2017), revealing the presence of both *narG* and *napA* genes in all  
561 piezometers of the catchment, thus showing a potential for microbial nitrate reduction in all  
562 studied piezometers of the Plourhan site (data not shown). Spatio-temporal variations in  
563 gene abundance were highlighted according to the sampling time and location. This agrees  
564 with earlier results that showed a temporal variation in the abundance of denitrification genes  
565 in groundwater, and a wide-ranging spatial distribution of these genes in a single catchment  
566 ([Hernandez-del Amo et al., 2018](#)).

567 To complete the isotopic and molecular approaches for nitrate reduction characterization in  
568 samples collected in April 2017, the potential nitrate reduction activity of microbial  
569 communities sampled from several piezometers was measured in batch experiments, run  
570 under standardized conditions for denitrification. Nitrate reduction activity was found in all  
571 the tested wells (Figure 9C). This agrees with the quantification of functional genes that were  
572 also detected, albeit at different relative abundances, in all piezometers (Figure 9 A and B),  
573 showing a spatially widespread potential of the groundwater microbial communities for  
574 reducing nitrate. These results agree with earlier work, showing the wide distribution of  
575 microbial communities involved in denitrification in groundwater ([Hernandez-del Amo et al.,  
576 2018](#)). Batch experiments showed a high heterogeneity among the piezometers, as nitrate  
577 reduction rates can be high (Pz7 and Pz10) or low (Pz6 and Pz9). They also showed that the  
578 complete denitrification pathway occurred, as nitrite ( $\text{NO}_2^-$ ) and  $\text{N}_2\text{O}$  were detected as well  
579 (data not shown). This strongly suggested that a complete denitrification can occur in the  
580 different groundwater of the catchment provided that *in situ* conditions are favourable.



581  
 582 *Figure 9 : Microbiological and biomolecular analyses of water collected in piezometers at the Plourhan site in April*  
 583 *2017. A and B: Relative abundance of narG gene copies (A) and napA gene copies (B) involved in bacterial*  
 584 *nitrate reduction, determined with quantitative PCR. (C) Potential nitrate reduction activity measured in batch*  
 585 *experiments under standardized conditions for denitrification (for all piezometers, no nitrate reduction was*  
 586 *observed in abiotic flasks). Significant differences between conditions were searched for by means of the Kruskal-*  
 587 *Wallis non-parametric test ( $p>0.05$ ) and are mentioned as letters (a, b... f).*

588 Intermediate and high potential nitrate reduction rates found in batch experiments for Pz8 (at  
 589 two depths) and Pz10, respectively, agree with the denitrification activity showed by isotopic  
 590 data and the *narG* and *napA* genes abundance results found for these piezometers. The low  
 591 potential nitrate reductase activities found for Pz9 and SR1 also agree with the isotopic  
 592 results, suggesting no denitrification for Pz9. The results were inconclusive for SR1 as the  
 593 nitrate concentration was too low, and because of the low abundance of genes encoding the  
 594 nitrate reductase enzymes. The results from the batch experiments for these four waters thus  
 595 agreed with the isotopic and molecular approaches.

596 However, no relation was found for the other piezometers. For Pz3 and Pz7, intermediate to  
 597 high activity was measured in batch experiments, but isotopic and molecular approaches  
 598 both suggested a low nitrate reduction potential. For Pz6, whereas the isotopic and  
 599 molecular approaches suggested nitrate reduction activity and a potential for such activity,  
 600 respectively, batch experiments only showed a weak nitrate reduction potential. These  
 601 differences could be due to unsuitable *in situ* conditions for denitrification compared to batch  
 602 experiments, in the case where batch experiments showed a high potential, but no nitrate  
 603 reduction was detected using isotopes. Another explanation might be that the *in situ* nitrate

604 reduction, shown by isotopic work is actually ancient, explaining why only a weak activity was  
605 detected in batch experiments.

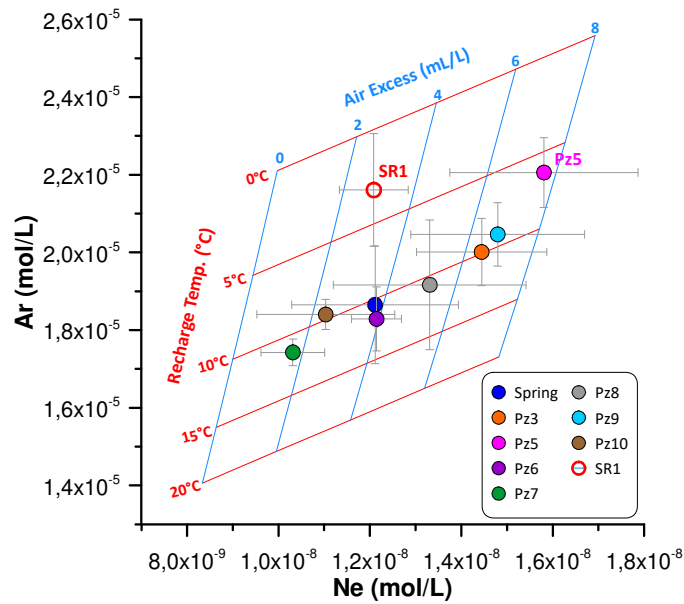
606 Therefore, according to geochemistry, isotopic tools and/or biomolecular characterization,  
607 the Pz5, PZ9 and SR1 wells highlight different water origins and/or mechanisms than in other  
608 piezometers. This is further investigated in the following section.

609

#### 610 4.4 Groundwater residence time assessment: CFCs, SF<sub>6</sub> and noble 611 dissolved gases

612 Dissolved gases (CFCs and SF<sub>6</sub>) were analysed during the two sampling periods (2009-2011  
613 and 2016-2018), to assess the groundwater residence time and the local aquifer dynamics  
614 (Table S3, Supplementary material). In this type of aquifer, the exponential model—reflecting  
615 a diffuse recharge at the catchment scale resulting in a mixture of old and young  
616 groundwater components at the outlet—generally is the most appropriate one. Here,  
617 however, the binary mixing model, that mixes different reservoirs, could be also suitable for  
618 reflecting the structure of the basement aquifer, consisting of fractured bedrock overlain by a  
619 weathered layer.

620 The Spring samples appear to be systematically contaminated with CFC-11 and CFC-12.  
621 However, as CFCs have been used worldwide in a wide range of activities, this type of  
622 contamination is common near urban areas or landfills (Höhener et al., 2003) and both  
623 tracers are unsuitable for dating purposes. Only CFC-113 and SF<sub>6</sub> can be used, thus  
624 increasing the uncertainty associated with estimating a mean residence time. According to  
625 the chemical characteristics of the Spring water and its relative stability during the year,  
626 groundwater dating tracers are interpreted with exponential model. Based on these two  
627 tracers, the mean  $\tau$  value (characteristic time needed for the two-thirds renewal of the aquifer  
628 water according to the exponential model) of the Spring waters is about  $20 \pm 5$  years. For the  
629 other piezometers (Pz) and borehole (SR1) in the catchment area, different groups can be  
630 used.



631  
 632 *Figure 10: Mean Neon versus Argon concentrations (mol/L) for each groundwater sample monitored during the*  
 633 *period 2016-2018 (n=2 for Pz10 to n=16 for the Spring). Blue and red lines represent the theoretical values from*  
 634 *solubility equations for an altitude of 100 m, a temperature between 0 to 20 °C and an excess air between 0 and 8*  
 635 *mL/L. Samples plotting in around the same red line have the same recharge temperature, but different excess air.*

636 A first group of samples is marked by lower recharge temperatures than the present-day one  
 637 of 11-12°C in Brittany (Ayraud et al., 2008). The noble-gas concentrations (Ar and Ne, Figure  
 638 10) measured in the SR1 borehole showed a recharge temperature of around 3-4 °C, i.e. 7 to  
 639 9 °C lower than the present-day one, indicating the presence of old groundwater in the  
 640 system that could be related to the last glaciation period of -19 to -17 ky (Aquilina et al.,  
 641 2015). In addition, the CFC and SF<sub>6</sub> measurements also indicate a long residence time  
 642 (mean 230±40 yr using an exponential model), with a possible contribution of a recent  
 643 component not exceeding 10 % that may reflect water inflow resulting from the pumping for  
 644 groundwater sampling (Figure 11).

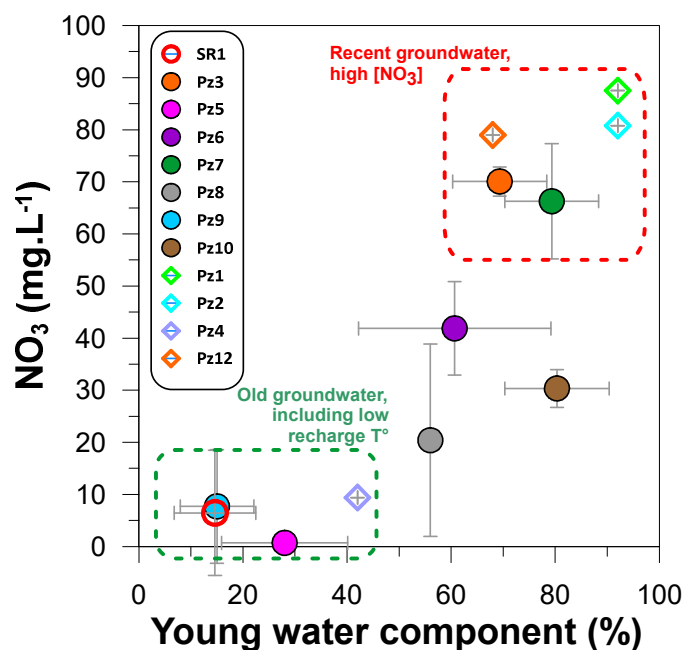
645 This recent component contained nitrate in some SR1 samples from the first sampling period  
 646 (2009), with NO<sub>3</sub> reaching 38 mg.L<sup>-1</sup> at 60 m depth *versus* 3.7 mg.L<sup>-1</sup> at 110 m depth. In  
 647 addition, during the second sampling period (2017-2018), an excess of 50 to 100% dissolved  
 648 N<sub>2</sub> was determined compared to Ne and Ar concentrations, with concentrations reaching  
 649 1.2.10<sup>-3</sup> to 1.4.10<sup>-3</sup> mol.L<sup>-1</sup> compared to 7.10<sup>-4</sup> to 8.10<sup>-4</sup> mol.L<sup>-1</sup> in the Spring samples This  
 650 may be a result from the denitrification of the incoming nitrate, no NO<sub>3</sub> being detected (<LQ)  
 651 during the second sampling period. In a second location, Pz5 tapping the saprolite and the  
 652 upper part of the fractured amphibolite, noble-gas analyses (n=2, Figure 10) also showed a  
 653 low recharge temperature of around 6 °C. While no nitrate was detected during the first  
 654 sampling period, about 1 mg.L<sup>-1</sup> was measured during the second sampling period, which  
 655 could corroborate the CFC-SF<sub>6</sub> analyses indicating between 70 and 85 % of old water (i.e.

656 CFC-SF<sub>6</sub> free), and thus a small contribution of recent water possibly enriched in nitrate  
657 (Figure 11).

658 Above, we also pointed out a relatively high Cl concentration of up to 72 mg.L<sup>-1</sup>, i.e. the  
659 highest concentration in the studied area (except Pz12 with both high Cl and NO<sub>3</sub>  
660 concentrations). An anthropogenic Cl contribution is unlikely as there is no nitrate and no  
661 denitrification process was detected. Pz5 samples are the only ones with a Na/Cl ratio close  
662 to that of seawater (Figure 5A). Combining the low recharge temperature, the absence of  
663 nitrate and the relatively high Cl concentration considered to be natural, this sampling point  
664 could reflect the legacy of marine transgressions over the past 5 millions years. Armandine  
665 Les Landes et al. (2015) considered that Cl of marine origin, not supplied by precipitation (>  
666 40 mg L<sup>-1</sup>) is likely related to marine transgressions that flooded the Armorican Massif since  
667 the Messinian. The large quantities of Cl injected during each transgression were then  
668 diluted by meteoric recharge after the end of the transgression period. This includes  
669 recharge during the last glaciation, shown by a low recharge temperature indicated by noble  
670 gases. In Pz5 at 18 m depth, the water comes from the upper part of the amphibolite  
671 basement and from the lower part of the overlying weathered material. This old water,  
672 preserved from anthropogenic impact, is disconnected from the groundwater feeding the  
673 Spring about 500 m distant, relatively disconnected from present day recharge, and only  
674 remobilized by pumping for sampling.

675 A second group, represented by Pz9, has a long mean residence time of over 60 years  
676 (Figure 11) , with a large proportion (80-90%) of old water and no CFC-SF<sub>6</sub>, but no evidence  
677 of low recharge temperatures. These waters thus appear to be younger than the ones of Pz5  
678 and SR1, but old enough not to have received anthropogenic nitrate.

679 The other groundwater samples have apparent ages of about 30 years, such as Pz10 and  
680 Pz3. Pz6 shows a variability between the two samples analysed for dating purposes. This  
681 can reflect mixing in various proportions between old and present-day waters (Figure 11)  
682 according to the period of the hydrological cycle, the apparent age being slightly older in May  
683 2018 than in October 2017. This variability was also observed for the major elements, which  
684 is typical of the sandstone and pelite aquifer that has different aquifer dynamics than the  
685 amphibolite aquifer. Pz7 has a high SF<sub>6</sub> contamination; based on the other tracers, the  
686 waters could correspond to a mixing between a large proportion of recent water (70-80%)  
687 and a 30-40-years old water.



688

689 *Figure 11: Mean NO<sub>3</sub> concentrations versus the mean percentage of the young-water component in each*  
 690 *groundwater sample of the study area.*

691 Such different groundwater residence times are known from other parts of Brittany.  
 692 Evidence of past climatic and geological event was found in groundwater from Lanleff  
 693 monitoring station < 10km west of Plourhan (Armandine Les Landes et al., 2015) and in  
 694 various other parts of Brittany by Aquilina et al. (2015). Most shallow groundwaters at a  
 695 regional scale, however, is strongly impacted by anthropogenic activity and has mean  
 696 apparent residence times of 10 to 30 years (Ayraud et al., 2008). All earlier studies studied  
 697 different regions, which raises questions about the functioning and connectivity of the aquifer  
 698 systems studied, questions that might be answered by detailed geological studies of the  
 699 sites.

700

## 701 5 Conclusions and perspectives

702

703 The Plourhan catchment (~100 ha) contains a main spring that still exceeds the limit of 50  
 704 mg/L NO<sub>3</sub> despite the numerous remedial measures implemented since the 1990s. We  
 705 investigated the catchment with complementary and robust geological and hydrogeological  
 706 approaches, better to constrain the driving parameters of nitrate transfer and distribution in  
 707 groundwater, and thus to improve our understanding of how the hydrosystem functions.

708 First, geochemical water sampling over about 10 years showed a quite high variability in  
 709 groundwater quality: (1) a temporal variability especially regarding nitrate and (2) a spatial  
 710 variability despite the small size of the catchment. Though a link with agricultural practices

711 and land use is one of the key factors controlling nitrate fate in groundwater, other factors  
712 must be considered as well, such as the hydro-biochemical functioning of the aquifer system,  
713 which can also largely control water quality.

714 Secondly, the study of nitrate isotopes (N and O) clearly demonstrated denitrification in  
715 some piezometers of the catchment area. Such processes were generally demonstrated by  
716 microbiology and molecular biology studies, highlighting the presence of functional genes  
717 involved in denitrification as well as the capacity of the groundwater microbial community for  
718 denitrifying when *in situ* anoxic and/or nutritive conditions are favourable. Other groundwater  
719 samples had low nitrate contents, even below the quantification limit, without any  
720 denitrification process occurring. Study of the average groundwater residence time, based on  
721 dissolved CFCs and SF<sub>6</sub> and on rare gases; locally discovered old waters, particularly in  
722 nitrate-free piezometers, demonstrating that such waters never received any anthropogenic  
723 nitrate. One piezometer contained old water, with a recharge temperature well below the  
724 current average temperature in the area, reflecting water from the last glaciation period (-19  
725 to -17 ky).

726 Third, the presence of such very old groundwater in the catchment area, raises questions  
727 about the structure of the aquifer system at the scale of the recharge area. The detailed  
728 geological and geophysical work, especially with electric tomography profiles, led to  
729 improvement of the local structural model. A large number of compartments delimited by  
730 faults was shown to exist, as was a highly variable thickness of soil and weathered rock in  
731 the study area. This better understanding of the geological structure has shown the  
732 heterogeneity of the hydrosystem, where some compartments appear to be disconnected  
733 from the general groundwater flow. This may explain the presence of old residual  
734 groundwater not affected by the agricultural activity in the catchment.

735 The Plourhan site has shown the relevance and necessity of using an integrated approach  
736 for significantly improving our knowledge in terms of the functioning of complex  
737 hydrosystems—such as basement ones— and its impact on groundwater quality. This  
738 approach can be advantageously applied to other sites, especially in basement domains  
739 where denitrification processes can deeply modify the local water quality, and where the  
740 geological structure may be quite complex. The various methods of such an approach can  
741 be implemented independently, and successively, steered by gradually improving  
742 knowledge, or in a coupled manner as done here. The understanding of hydrodynamic  
743 functioning *sensu lato* is as important as that of nitrate reduction. Both are paramount for  
744 implementing the most relevant programmes of measures (as required by the European  
745 Water Framework Directive; Fifth WFD and FD Implementation Reports, 2019), for

746 recovering a good water quality and assessing the effectiveness of such measures and  
747 methods, notably by considering the timeframe between implementation of the measures  
748 and their impact on groundwater quality.

749

## 750 **6 Acknowledgments**

751 The French Loire-Bretagne Water Agency (AELB) together with the BRGM financially  
752 supported this study through the POLDIF Research project led by N. Baran. The authors  
753 thanks Florian Koch, Benjamin Maurice and Mickael Charron for their precious assistance in  
754 the field, Marine Gremont for her synthesis of the measures for recovering water quality. All  
755 colleagues from the BRGM Labs involved in the data production are thanked for their  
756 valuable work. Jean-Michel Schroetter is warmly thanked for the many fruitful discussions on  
757 the local geological settings and how they can govern water circulations and water quality. E.  
758 Petelet-Giraud addresses special thanks to Gilles L. and Christophe G. for their fruitful  
759 comments on figure 8. We are grateful to Dr. H.M. Kluijver for proofreading and editing the  
760 English text.

761

762

## 763 **7 References**

- 764 Aeschbach-Hertig W., Solomon D.K. (2013) Noble Gas Thermometry in Groundwater Hydrology. *In:*  
765 Burnard P. (eds) The Noble Gases as Geochemical Tracers. Advances in Isotope Geochemistry.  
766 Springer, Berlin, Heidelberg.
- 767 Aquilina, L., Vergnaud-Ayraud, V., Labasque, T., Bour, O., Molénat, J., Ruiz, L., de Montety, V., De  
768 Ridder, J., Roques, C., Longuevergne, L., 2012. Nitrate dynamics in agricultural catchments deduced  
769 from groundwater dating and long-term nitrate monitoring in surface- and groundwaters. *Sc. Tot. Env.*  
770 435–436, 167-178. <https://doi.org/10.1016/j.scitotenv.2012.06.028>.
- 771 Aquilina, L., Vergnaud-Ayraud, V., Armandine Les Landes, A., Pauwels, H., Davy, Ph., Petelet-Giraud,  
772 E., Labasque, T., Roques, C., Chatton, E., Bour, O., Ben Maamar, S., Dufresne, A., Khaska, M., Le  
773 Gal La Salle, C., Barbecot, F., 2015. Impact of climate changes during the last 5 million years on  
774 groundwater in basement aquifers. *Nature Scientific Rep.* 5, 14132; doi: 10.1038/srep14132.
- 775 Aquilina, L., Roques, C., Boisson, A., Vergnaud-Ayraud, V., Labasque, T., Pauwels, H., Petelet-  
776 Giraud, E., Pettenati, M., Dufresne, A., Bethencourt, L., Bour, O., 2018. Autotrophic denitrification  
777 supported by biotite dissolution in crystalline aquifers (1): New insights from short-term batch  
778 experiments. *Sci. Total Environ.* 619–620, 842–853. <https://doi.org/10.1016/j.scitotenv.2017.11.079>
- 779 Aravena, R., Robertson, W.D., 1998. Use of multiple isotope tracers to evaluate denitrification in  
780 groundwater: study of nitrate from a large-flux septic system plume. *Ground Water* 36, 975–982.
- 781 Armandine Les Landes, A., Aquilina, L., Davy, P., Vergnaud-Ayraud, V., Le Carlier, C., 2015.  
782 Timescales of regional circulation of saline fluids in continental crystalline rock aquifers (Armorican  
783 Massif, western France). *Hydrol. Earth Syst. Sci.* 19, 1413–1426. <https://doi.org/10.5194/hess-19-1413-2015>  
784

- 785 Ayraud, V., Aquilina, L., Labasque, T., Pauwels, H., Molenat, J., Pierson-Wickmann, A.C., Durand, V.,  
786 Bour, O., Tarits, C., Le Corre, P., Fourre, E., Merot, Ph., Davy, Ph., 2008. Compartmentalization of  
787 physical and chemical properties in hard-rock aquifers deduced from chemical and groundwater age  
788 analyses. *Appl. Geochem.* 23, 2686–2707.
- 789 Baran, N., Richert, J., Mouvet, C., 2007. Field data and modelling of water and nitrate movement  
790 through deep unsaturated loess. *J. Hydrol.* 345, 27-37.
- 791 Barrett, M., Jahangir, M., Lee, C., Smith, C., Bhreathnach, N., Collins, G., Richards, K., O’Flaherty, V.,  
792 2013. Abundance of denitrification genes under different piezometer depths in four Irish agricultural  
793 groundwater sites. *Environ. Sci. Pollut. Res.* 20, 6646-6657.
- 794 Belle, P., Lachassagne, P., Mathieu, F., Barbet, C., Brisset, N., Gourry, J.C., 2019. Characterization  
795 and location of the laminated layer within hard rock weathering profiles from electrical resistivity  
796 tomography: implications for water well siting. *Geol. Soc. London, Spec. Publ.* 479, 187-205.  
797 <https://doi.org/10.1144/SP479.7>
- 798 Berner-Kay, E.K., Berner, R.A., 1987. *The Global Water Cycle Geochemistry and Environment.*  
799 Prentice-Hall, Englewood Cliffs, 397 pp.
- 800 Böttcher J., Strebel O., Voerkelius S., Schmidt H.L., 1990. Using isotope fractionation of nitrate-  
801 nitrogen and nitrate-oxygen for evaluation of microbial denitrification in a sandy aquifer, *J. Hydrol.* 114,  
802 413.
- 803 Bru, D., Sarr, A., Philippoy, L., 2007. Relative abundances of proteobacterial membrane-bound and  
804 periplasmic nitrate reductases in selected environments. *Appl. Environ. Microbiol.* 73, 5971-5974.
- 806 Buchwald, C., Casciotti, K. L., 2010. Oxygen isotopic fractionation and exchange during bacterial  
807 nitrite oxidation. *Limnol. Oceanogr.* 55, 1064-1074.
- 808 Busenberg, E., Plummer, L.N., 1992. Use of chlorofluorocarbons (CCL3F and CCL2F2) as hydrologic  
809 tracers and age-dating tools - the alluvium and terrace system of Central Oklahoma. *Wat. Res. Res.*  
810 28, 2257-2283. doi: 10.1029/92WR01263.
- 811 Cabrol, L., Quéméneur, M., Misson, B., 2017. Inhibitory effects of sodium azide on microbial growth in  
812 experimental resuspension of marine sediment. *J. Microbiol. Meth.* 133, 62-65.
- 814 Ceballos, E., Margalef-Martí, R., Carrey, R., Frei, R. Otero, N., Soler, A., Ayora, C., 2020.  
815 Characterisation of the natural attenuation of chromium contamination in the presence of nitrate using  
816 isotopic methods. A case study from the Matanza-Riachuelo River basin, Argentina. *Sc. Tot. Env.* 699,  
817 134331.
- 818 Chang C.C.Y., Langston J., Riggs M., Campbell D.H., Silva S.R., Kendall C., 1999. A method for  
819 nitrate collection for  $\delta^{15}\text{N}$  and  $\delta^{18}\text{O}$  analysis for water with low nitrate concentrations, *Can. J. Fish.*  
820 *Aquat. Sci.* 56, 1856.
- 822 Chatton, E.; Aquilina, L.; Petelet-Giraud, E.; Cary, L.; Bertrand, G.; Labasque, T.; Hirata, R., Martins,  
823 V., Montenegro, S., Vergnaud, V., Aurouet, A., Kloppmann, W., Pauwels, H., 2016. Glacial recharge,  
824 salinization and anthropogenic contamination in the coastal aquifers of Recife (Brazil). *Sc. Tot. Env.*  
825 569–570, 1114–1125.
- 826 Chen, F., Jia, G., Chen, J., 2009. Nitrate Sources and Watershed Denitrification Inferred from Nitrate  
827 Dual Isotopes in the Beijiang River, South China. *Biogeochem.* 94, 163-174.
- 828 Comte, J.C., Cassidy, R., Nitsche, J., Offerdinger, U., Pilatova, K., Flynn, R., 2012. The typology of  
829 Irish hard-rock aquifers based on an integrated hydrogeological and geophysical approach.  
830 *Hydrogeol. J.* 20, 1569-1588. <https://doi.org/10.1007/s10040-012-0884-9>
- 831 Critchley, K., Rudolph, D.L., Devlin, J.F., Schillig, P.C., 2014. Stimulating in situ denitrification in an  
832 aerobic, highly permeable municipal drinking water aquifer. *J. Contam. Hydrol.* 171, 66–80.

- 836 Dewandel, B., Lachassagne, P., Wyns, R., Maréchal, J.C., Krishnamurthy, N.S., 2006. A generalized  
837 3-D geological and hydrogeological conceptual model of granite aquifers controlled by single or  
838 multiphase weathering. *J. Hydrol.* 330, 260-284. <https://doi.org/10.1016/j.jhydrol.2006.03.026>
- 839 Egal, E., Guennoc, P., Le Goff, E., Thiéblemont, D., Houlgatte, E., Augris, C., Hamon, D., Lebreton, P.,  
840 Hallégouët, B., 1996. Carte géol. France (1/50 000), feuille Pontrieux—Étables-sur-Mer (204).  
841 Orléans: BRGM
- 842 Egal, E., Le Goff, E., Guennoc, P., Lebreton, P., Thiéblemont, D., Hallégouët, B., Houlgatte, E., Callier,  
843 M., Carn, A., 1995. Notice explicative, carte géologique de la France (1/50 000), feuille Pontrieux -  
844 Étables-sur-Mer (204). Orléans: BRGM, 194 p..
- 845 European Commission, 1991. Council Directive 91/676/EEC of 12 December 1991 concerning the  
846 protection of waters against pollution caused by nitrates from agricultural sources. *Official Journal L*  
847 375, 31/12/1991.
- 848 European Commission, 2000. Directive 2000/60/EC of the European Parliament and of the Council  
849 establishing a framework for the Community action in the field of water policy. *EU Water Framework*  
850 *Directive (WFD)*. *Official Journal of the European Community* L327.
- 851 European Commission, 2006. Directive 2006/118/EC of the European Parliament and of the Council of  
852 12 December 2006 on the protection of groundwater against pollution and deterioration. *EU*  
853 *Groundwater Directive (GWD)*. *Official Journal of the European Union* L 372.
- 854 European Commission, 2018. Report from the Commission to the Council and the European  
855 Parliament on the implementation of Council Directive 91/676/EEC concerning the protection of waters  
856 against pollution caused by nitrates from agricultural sources based on Member State reports for the  
857 period 2012–2015. SWD (2018) 246 final. Available at: [https://ec.europa.eu/environment/water/water-](https://ec.europa.eu/environment/water/water-nitrates/reports.html)  
858 [nitrates/reports.html](https://ec.europa.eu/environment/water/water-nitrates/reports.html).
- 859 Fenech C., Rock L., Nolan K., Tobin J., Morrissey A., 2012. The potential for a suite of isotope and  
860 chemical markers to differentiate sources of nitrate contamination: A review. *Wat. Res.* 46, 2023-2041.
- 861 Fifth Water Framework Directive Implementation Report – assessment of the second River Basin  
862 Management Plans and the first Floods Directive Implementation Report – assessment of the first  
863 Flood Risk Management Plans, 2019. Available at: [https://ec.europa.eu/environment/water/water-](https://ec.europa.eu/environment/water/water-framework/impl_reports.htm)  
864 [framework/impl\\_reports.htm](https://ec.europa.eu/environment/water/water-framework/impl_reports.htm).
- 865 Granger, J., Wankel, S.D., 2016. Isotopic overprinting of nitrification on denitrification as a ubiquitous  
866 and unifying feature of environmental nitrogen cycling. *Proc. Natl. Acad. Sci.* 113:E6391–E6400.  
867 <https://doi.org/10.1073/pnas.1601383113>
- 868 Heaton, T.H.E., Vogel, J.C., 1981. Excess air in groundwater. *J. Hydrol.* 50, 201-216.
- 869 Hernández-del Amo, E., Menció, A., Gich, F., Mas-Pla, J., Baneras, L., 2018. Isotope and microbiome  
870 data provide complementary information to identify natural nitrate attenuation processes in  
871 groundwater. *Sci. Tot. Environ.* 613-614, 579-591.
- 872 Höhener, P., Werner, D., Balsiger, C., Pasteris, G., 2003. Worldwide occurrence and fate of  
873 chlorofluorocarbons in groundwater. *Critic. Rev. Env. Sc. and Techn.* 33, 1–29.
- 874 IAEA, 2006. Use of Chlorofluorocarbons in Hydrology: A Guidebook. STI/PUB 1238, IAEA, Vienna.
- 875 Kendall, C., 1998. Tracing Nitrogen Sources and Cycling in Catchments (Chapter 16). *In: Isotope*  
876 *Tracers in Catchment Hydrology* (Eds C. Kendall, J.J. McDonnell), 1<sup>st</sup> Ed. pp. 519–576. Elsevier,  
877 Amsterdam. Paperback ISBN: 9780444501554.
- 878 Kendall, C., Aravena, R., 2000. Nitrate Isotopes in Groundwater Systems. *In: Environmental Tracers in*  
879 *Subsurface Hydrology* (Eds P. Cook, A. Herczeg), pp. 261–297. Kluwer Academic Publ., Boston, MA.

- 880 Kendall, C., Elliott, E.M, Wankel, S.D., 2007. Chapter 12: Tracing Anthropogenic Inputs of Nitrogen to  
881 Ecosystems. In: Stable Isotopes in Ecology and Environmental Science, Robert Michener and Kate  
882 Lajtha (eds.), 2<sup>nd</sup> edition.
- 883 Kloppmann, W., 2003. Etude isotopique de la pollution azotée de la nappe d'Alsace entre Sierentz et  
884 Ottmarsheim. Rapport BRGM BRGM/RP-52331 -FR, 69 p.
- 885 Kumar, S., Nicholas, D.J.D., Williams, E.H., 1983. Definitive <sup>15</sup>N NMR evidence that water serves as a  
886 source of 'O' during nitrite oxidation by *Nitrobacter agilis*. FEBS Lett. 152, 71-74.
- 887 Labasque, T., Aquilina, L., Vergnaud, V., Barbecot, F., 2014. Inter-laboratory comparison of the  
888 analyses of sulphur hexafluoride (SF<sub>6</sub>) and three chlorofluorocarbons (CFC-11, -12 and -113) in  
889 groundwater and an air standard. Appl. Geochem. 50, 118–129.  
890 <http://dx.doi.org/10.1016/j.apgeochem.2014.03.009>
- 891 Loke, M.H., 2013. Tutorial : 2-D and 3-D electrical imaging surveys. Geotomo Softw. Malaysia 127.
- 892 Lu, L., Cheng, H., Pu, X., Liu, X., Cheng, Q., 2015. Nitrate behaviors and source apportionment in an  
893 aquatic system from a watershed with intensive agricultural activities. Environ. Sci.: Proc. Imp. 17,  
894 131-144
- 895 Matoszewski, P., Zuber, A., 1996. Lumped parameter models for the interpretation of environmental  
896 tracer data. In: Manual on Mathematical Models in Isotope Hydrogeology. IAEA-TECDOC-910, ISSN  
897 1011-4289. International Atomic Energy Agency, Vienna, pp. 9-58.
- 898 Margalef-Marti, R., Carrey, R., Viladés, M., Jubany, I., Vilanova, E., Grau, R., Soler, A., Otero, N.,  
899 2019. Use of nitrogen and oxygen isotopes of dissolved nitrate to trace field-scale induced  
900 denitrification efficiency throughout an in-situ groundwater remediation strategy. Sci. Total Env. 686,  
901 709–718.
- 902 Mariotti, A., Landreau, A., Simon, B., 1988. <sup>15</sup>N isotope biogeochemistry and natural denitrification  
903 process in groundwater: application to the chalk aquifer of northern France. Geochim. Cosmochim.  
904 Acta 52, 1869–1878.
- 905 Mengis, M., Schiff, S.L., Harris, M., et al., 1999. Multiple geochemical and isotopic approaches for  
906 assessing ground water NO<sub>3</sub><sup>-</sup> elimination in a riparian zone. Ground Water, 37, 448–457.
- 907 Mengis, M., Walther, U., Bernasconi, S.M., Wehrli, B., 2001. Limitations of using delta <sup>18</sup>O for the  
908 source identification of nitrate in agricultural soils. Environ Sci Technol., 35, 1840-4.
- 909 Meybeck, M., 1983. Atmospheric inputs and river transport of dissolved substances. IAHS publ. 141,  
910 173-192.
- 911 Négrel, Ph, Guerrot, C., Millot, R., 2007. Chemical and strontium isotope characterisation of rainwater  
912 in France. Isot. Environ. Health Stud. 43,179–196.
- 913 Otero, N., Torrentó, C., Soler, A., Menció, A., Mas-Pla, J., 2009. Monitoring groundwater nitrate  
914 attenuation in a regional system coupling hydrogeology with multi-isotopic methods: the case of Plana  
915 de Vic (Osona, Spain). Agric. Ecosyst. Environ. 133,103–113.
- 916 Pauwels, H., Kloppmann, W., Foucher, J.C., Martelat, A., Fritsche, V., 1998. Field tracer test for  
917 denitrification in a pyrite-bearing schist aquifer. Appl. Geochem. 13, 767–778.
- 918 Pauwels, H., Foucher, J.C., Kloppmann, W., 2000. Denitrification and mixing in a schist aquifer:  
919 influence on water chemistry and isotopes. Chem. Geol. 168, 307–324.
- 920 Petelet-Giraud E., Pettenati M., Aquilina L., Pauwels H., Kloppmann W., Boisson A., Chatton E.,  
921 Mathurin F., 2017. Denitrification processes in a schist aquifer: multi-isotope constraint applied to a  
922 field tracer test. Proc. 12<sup>th</sup> Int. Symp. Appl. Isot. Geochem. (AIG-12), 18-22 Sep 2017, Copper  
923 Mountain (Colorado), USA. 4 pages, available at:  
924 [http://www.appliedisotopegeochemistry.org/abstracts/AIG-12/Petelet-](http://www.appliedisotopegeochemistry.org/abstracts/AIG-12/Petelet-Giraud%20et%20al.%20Denitrification%20processes%20in%20a%20schist%20aquifer.pdf)  
925 [Giraud%20et%20al.%20Denitrification%20processes%20in%20a%20schist%20aquifer.pdf](http://www.appliedisotopegeochemistry.org/abstracts/AIG-12/Petelet-Giraud%20et%20al.%20Denitrification%20processes%20in%20a%20schist%20aquifer.pdf).

- 926 Puig, R., Soler, A., Widory, D., Mas-Pla, J., Domenech, C., Otero, N., 2017. Characterizing sources  
927 and natural attenuation of nitrate contamination in the Baix Ter aquifer system (NE Spain) using a  
928 multi-isotope approach. *Sci. Total Environ.* 580, 518–532.  
929 <https://doi.org/10.1016/j.scitotenv.2016.11.206>
- 930 Reynolds, J.M., 2011. *An Introduction to Applied and Environmental Geophysics*. John Wiley & Sons.
- 931 Sebilo, M., Mayer, B., Nicolardot, B., Pinay, G., Mariotti, A., 2013. Long-term fate of nitrate fertilizer in  
932 agricultural soils. *PNAS* 110, 18185–18189.
- 933 Silva S.R., Kendall C., Wilkinson D.H., Ziegler A.C., Chang C.C.Y., Avanzino R.J, 2000. A new  
934 method for collection of nitrate from fresh water and the analysis of nitrogen and oxygen isotope ratios,  
935 *J. Hydrol.* 228, 22.
- 936 Stein, L.Y., Klotz, M.G., 2016. The Nitrogen Cycle. *Current Biology* 26, R94-R98, February 8.
- 937 Sugisaki, R., Taki, K., 1987. Simplified analyses of He, Ne and Ar dissolved in natural-waters.  
938 *Geochem. J.* 21, 23-27.
- 939 Widory, D., Petelet-Giraud, E., Négrel, P., Ladouche, B., 2005. Tracking the sources of nitrate in  
940 groundwater using coupled nitrogen and boron isotopes: a synthesis. *Environ. Sci. Technol.* 39, 539–  
941 548. <https://doi.org/10.1021/es0493897>
- 942 Widory, D., Petelet-Giraud, E., Brenot, A., Bronders, J., Tirez, K., Boeckx, P., 2013. Improving the  
943 management of nitrate pollution in water by the use of isotope monitoring: the  $\delta^{15}\text{N}$ ,  $\delta^{18}\text{O}$  &  $\delta^{11}\text{B}$   
944 triptych. *Isotopes in Environmental & Health Studies* 49, 29-47.
- 945 Zhang, Y., Shi, P., Song, J., Li, Q., 2019. Application of nitrogen and oxygen isotopes for source and  
946 fate identification of nitrate pollution in surface water: A review. *Applied Sciences* 9, 18.  
947 <https://doi.org/10.3390/app9010018>.
- 948